European Polymer Journal 201 (2023) 112553

Contents lists available at ScienceDirect

European Polymer Journal

journal homepage: www.elsevier.com/locate/europolj

Review

Facilitating the additive manufacture of high-performance polymers through polymer blending: A review

Dejana Pejak Simunec *, Johnson Jacob, Ahmad E.Z. Kandjani, Adrian Trinchi, Antonella Sola

Commonwealth Scientific and Industrial Research Organisation (CSIRO), Manufacturing Business Unit, Research Way, Melbourne, VIC 3168, Australia

ARTICLE INFO

Keywords:
Additive manufacturing
High performance polymers
FFF, Fused Filament Fabrication
FDM

ABSTRACT

Fused Filament Fabrication (FFF, a.k.a. fused deposition modeling, FDM) is presently the most widespread material extrusion (MEX) additive manufacturing technique owing to its flexibility and robustness. Nonetheless, it remains underutilized in load-bearing applications, as often seen in aerospace, automotive and biomedical industries. This is largely due to the processing challenges associated with high performance polymers (HPPs) like poly-ether-ether-ketone (PEEK) or polyetherimide (PEI). Compared with commercial-grade plastics such as polylactic acid (PLA), parts produced with HPPs have outstanding mechanical properties and thermal stability. However, HPPs have bulkier chemical structures and stronger intermolecular forces than common FFF feedstock materials, and this results in much higher printing temperatures and greater melt viscosities. The demanding processing requirements of HPPs have thus impaired their adoption within FFF. Polymer blending, which consists in properly mixing HPPs with other thermoplastics, makes it possible to alleviate these printing issues, while also providing additional advantages such as improved tensile strength and reduced friction. Further to this, manipulating the crystallisation processes of HPPs mitigates distortion or warping upon printing. This review explores some emerging trends in the field of HPP blends and how they address the challenges of excessive melt viscosity, polymer crystallization, moisture uptake, and part shrinkage in 3D printing. Also, the various structural/mechanical/chemical enhancements that are afforded to FFF parts through HPP blending are critically analysed based on recent examples from the literature. Such insights will not only aid researchers in this field, but also facilitate the development of novel, 3D printable HPP blends.

1. Introduction

High performance polymers (HPPs) in additive manufacturing (AM) have generated significant interest for the design of high strength/low weight parts with complicated or bespoken geometries in demanding biomedical, aerospace and automotive applications [1]. The added benefit of reduced corrosion susceptibility means these materials are a suitable replacement for parts traditionally made from metals. For example, HPPs have been used in the production of the tank heat shields of the Ducati Panigale V4 R Superbike [2].

The most important form of AM that enables the production of HPP parts is Fused Filament Fabrication (FFF). FFF, commercially referred to as Fused Deposition Modelling, or FDM (after Stratasys trademark), belongs to the material extrusion category, MEX, according to ISO/ASTM 52900:2021 [3]. Unlike other AM technologies, FFF has been verified for its suitability in microgravity or zero gravity environments [4,5] and can therefore be used in challenging scenarios such as aboard the International Space Station, ISS, where HPPs play a crucial role owing to their exceptional mechanical strength and stability. The FFF of HPPs is also being tested in lunar environments by the European Space Agency (ESA) [6].

In order to maximize the specific strength of HPP components obtained by FFF, current literature is focused on the effect of the printing parameters on the mechanical properties of the printed part. The effect of toolpath planning and post processing of HPP parts printed by FFF has also been examined [7]. Generally speaking, the results obtained for HPPs follow the same trends as those observed for commercial grade polymers. In terms of feedstock materials, research has been mainly addressed to poly-ether-ether-ketone (PEEK) [8], polyetherimide (PEI) [9], polyphenylene sulfide (PPS) and poly-ether-ketone-ketone (PEKK) [10]. Going a step further, some studies have delved into designing and printing composites using these polymers as the matrix combined with fillers and reinforcements like carbon fibres [11], carbon nanotubes and graphene nanoplatelets [12], and hydroxyapatite [13].

* Corresponding author.
E-mail address: Dejana.pejak@csiro.au (D.P. Simunec).

https://doi.org/10.1016/j.eurpolymj.2023.112553
Received 26 May 2023; Received in revised form 20 September 2023; Accepted 28 October 2023
Available online 7 November 2023

However, there are still substantial challenges that plague the utilization of HPPs in FFF. This is partly due to their bulkier chemical structures and stronger intermolecular forces compared with commercial thermoplastic feedstocks such as poly (lactic acid) (PLA) or acrylonitrile–butadienestyrene (ABS) [14]. The bulkier and stiffer chemical structure and the increased intermolecular attraction result in high viscosity materials that are significantly more difficult to extrude and print than conventional thermoplastics [15]. This often requires direct drive extruders or motors to be inbuilt within the printer in order to supply enough torque for extruding the melt. In addition, due to their much higher processing temperatures, HPPs need specific printers capable of reaching nozzle temperatures above 350 °C and fitted with metal print head casings and with a heated chamber [16].

In other "conventional" (i.e., not AM) melt processing techniques, like injection or compression moulding, a way to alleviate high temperature and viscosity issues in HPPs has been to combine these materials with one or more other thermoplastics to obtain polymer blends. Depending on the specific properties and the mutual miscibility of the constituents, these blends can affect specific interactions between polymer chains to induce a desired functional response. For example, Kumar, Mishra and Nandi [17] demonstrated that melt processing of PEEK can be facilitated by the addition of a small amount of PEI, as this reduces the melt viscosity as discussed in more detail in Section 6.1.2. Another desired effect may be mitigating shrinkage or part deformation upon cooling. This can be achieved, for instance, by blending miscible polyarylether constituents [18], as further explained in Section 5. Blending can even improve the tensile strength or other mechanical properties of HPPs. For example, PEEK can be blended with an (immiscible) liquid crystal polymer (LCP) to produce fibrous structures that reinforce the bulk polymer as demonstrated by Mehta and Isayev [18]. However, these studies have proved the usefulness of HPP blends in melt processing techniques like injection moulding (first patented in 1872) and compression moulding (invented in 1905), which have all been established long before FFF (ideated in 1988 by Scott and Lisa Crump).

Conceivably, there is still a significant gap in transferring the learnings about HPP blends from "conventional" melt processing to the more newly developed FFF printing. As thoroughly examined in the present review, the adoption of polymer blending in FFF holds the promise to greatly improve the printability of HPPs, as well as to ameliorate the mechanical and physical properties of the printed components. As such, this review aims to boost the utilization of HPPs within FFF through polymer blending, and to assist researchers in developing these polymers for demanding structural applications. To this end, the functioning mechanisms of FFF are introduced first, with a focus on the bonding mechanisms that are responsible for structural consolidation (Section 2.1), and on the polymer characteristics that affect printing by FFF (Section 2.2), especially when HPPs are used as feedstock materials. Then, Section 3 dives deeper into the definition and fundamental properties of HPPs, while also discussing the advantages and disadvantages of various approaches to facilitating their melt processing and hence to improving their printability. The state of the art in the FFF of HPPs is summarised in Section 4. Given the existing challenges associated with the FFF of HPPs, polymer blending is thus put forward as an effective solution. Accordingly, Section 5 examines the basic principles of polymer blending, and the different kinds of polymer blends that can be obtained according to the polymers' miscibility and crystallinity. As the main topic of this review, Section 6 examines the archival literature to dig out examples of polymer blends that have been developed to ameliorate the processability and improve the mechanical performance of HPPs in "conventional" melt processing techniques, whereas Section 7 specifically targets HPP blends that have already been demonstrated in FFF. In stark contrast to the dozens of examples available in conventional melt processing, just a handful of papers have explored the usefulness of polymer blending for FFF, which is further discussed in Section 8. Finally, relevant Conclusions are drawn in Section 9.

2. FFF printing

FFF is the process of 3D printing by melting and extruding a thermoplastic filament (feedstock) through a heated nozzle onto a build platform [19] (Fig. 1). The process begins with a 3D model that is sliced into thin multiple layers using specialized software such as g-code, which controls the movement of the print head in the X-Y plane. The computer-controlled print head contains the motors that supply driving force to push the filament downward into the liquefier, which heats the material to a melt state [20]. The thermoplastic material is thus heated, melted (or softened for amorphous materials) and deposited in a predetermined pattern based on the model's g-code. Upon deposition, the thermoplastic material cools and welds to the previously deposited strands [21]. The process is repeated in a layer-by-layer manner until the part is complete.

Ultimately, obtaining a high-quality part largely depends on having consistent deposition. To this aim, the feedstock material must flow out of the nozzle in a controlled way to reduce potential imperfections that could result in inadequate mechanical properties in the printed part [22]. In FFF, successful inter-layer and intra-layer bonding also plays a critical role in determining the mechanical properties and performance of the printed parts [23,24]. As detailed in the following paragraphs, the quality of interlayer bonding is influenced by various factors, including material properties, printing parameters, and post-processing conditions [25].

2.1. FFF bonding mechanism

Fig. 2 illustrates the bonding mechanism that occurs upon printing when the molten material contacts the previously deposited strands at the build plate. Successful bonding involves three key steps: 1) surface contact, 2) neck growth driven by surface tension, and 3) molecular diffusion and entanglement across the inter-strand interface. The bonding strength is predominantly influenced by the width of the neck (see Fig. 2) and the degree of molecular diffusion/entanglement occurring at the interface [26]. Typically, polymers with low molecular weight and high crystallinity tend to have weaker interlayer bonding, whereas those with high molecular weight and amorphous structures exhibit stronger interlayer bonding [27,28].

Sun et al. [29] defined "healing" as the molecular diffusion occurring at the interface between rasters, resulting in a partially welded structure. Polymer sintering, on the other hand, refers to the neck growth phenomenon driven by surface tension. Semi-crystalline polymers are typically sintered above their melting temperature (Tm). Likewise, amorphous polymers are sintered above their glass transition temperature (Tg). This is primarily due to polymer sintering being based on viscous flow mechanisms that require certain temperature-activated macromolecular chain mobility [30].

The strand-wise build-up strategy in FFF typically results in strongly anisotropic mechanical properties (refer to Fig. 2), which are dictated by the alignment of polymer chains along the printing direction, the weak interlayer bonding, and the presence of voids between the strands. Also, due to the weak strand-strand bonding and the possible presence of voids at strand junctions as illustrated in Fig. 2, the mechanical strength of FFF parts is generally lower than the corresponding parts produced by melt processing techniques such as injection and compression moulding. Levenhagen and Dadmun [31,32] leveraged the movement of fast diffusing short polymer chains to improve the interlayer adhesion and subsequently increase the mechanical strength of the printed parts. Recent studies have also demonstrated that both process control and polymer modification can enhance interface bonding in FFF parts [33]. Furthermore, post-processing through thermal annealing or cold plasma treatment may also improve interlayer bonding [34,35].

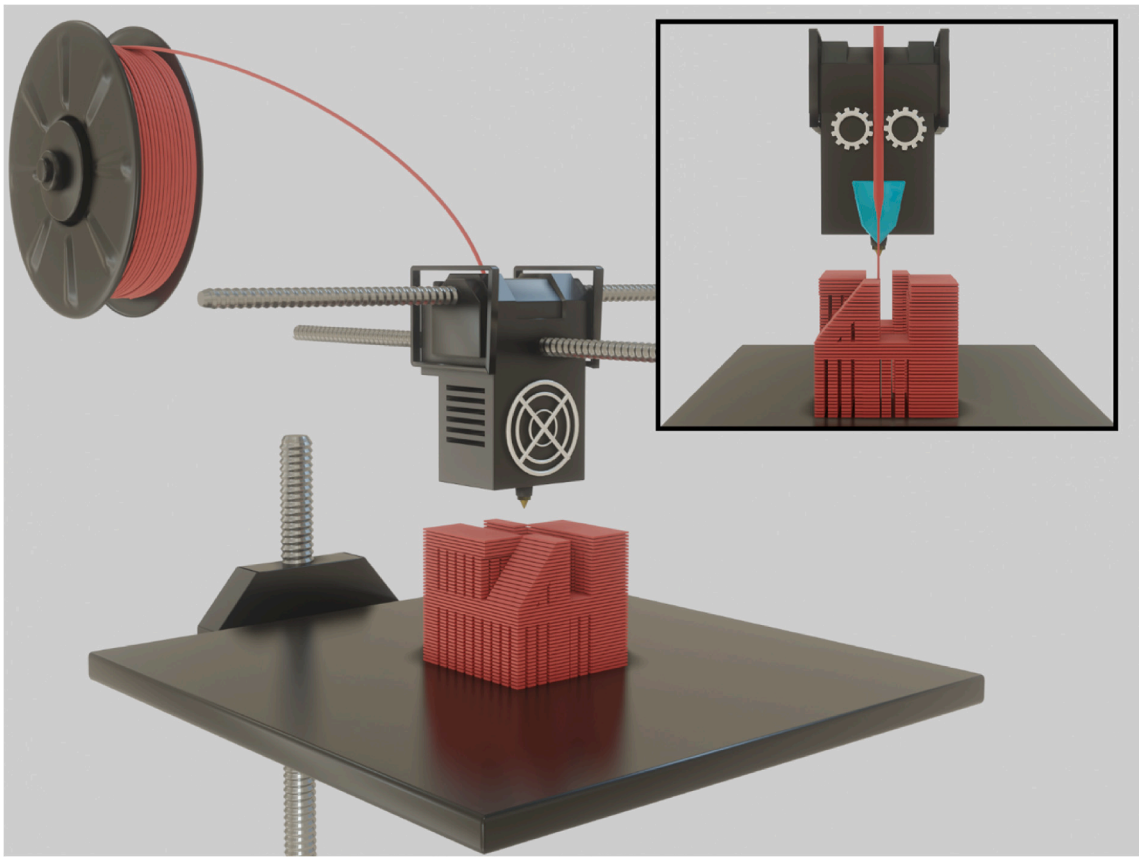

Fig. 1. Schematic diagram of the FFF printing process in a cartesian space (where the deposition plane is defined by X-Y axes, and the growth direction by Z axis). Feedstock is supplied as filament, heated, forced to flow through the nozzle by the feed rollers, and deposited onto the build platform (or previous layers). Once each layer is deposited, the build plate moves down along the z-axis.

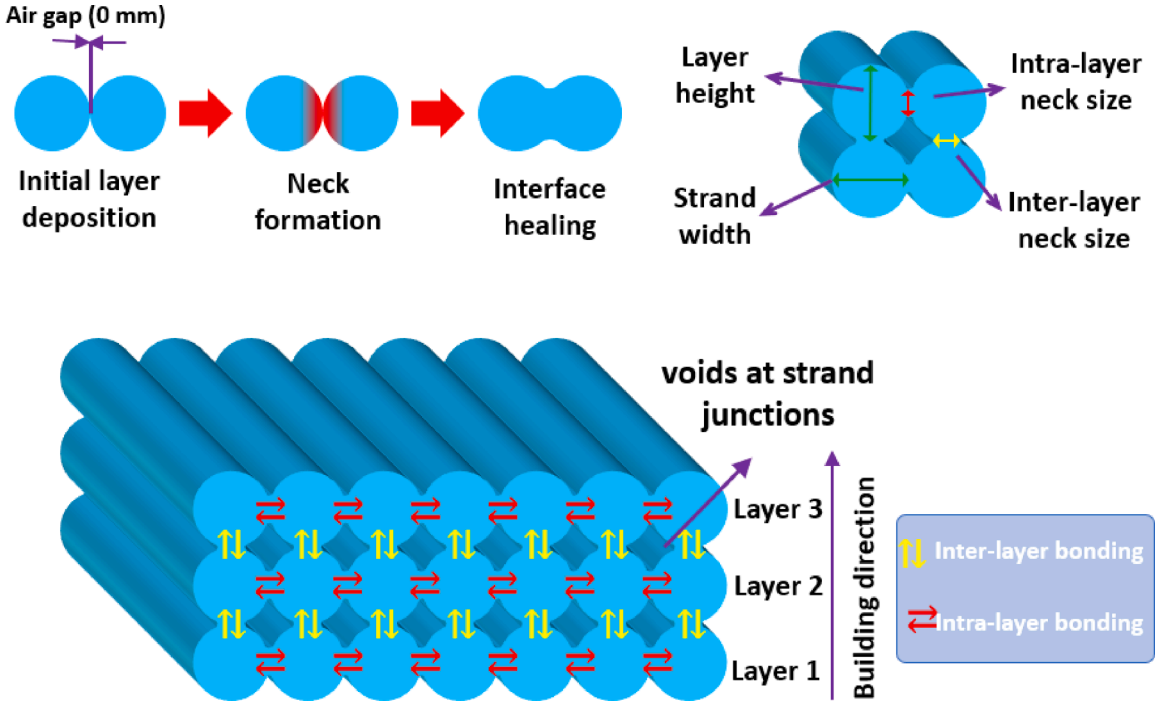

Fig. 2. Bond formation in the FFF process.

2.2. Polymer characteristics that affect FFF

Aside from the anisotropic and inferior mechanical properties of FFF parts relative to the bulk properties of the polymer, there are additional difficulties when HPPs are used as feedstock materials in FFF (Fig. 3). Firstly, the printing temperature of HPPs is much higher than that of commercial-grade polymers. As a result, the printing hardware must be engineered to be thermally resistant.

Most HPPs are semi-crystalline, with a fast crystallisation rate. This may impair the achievement of strong inter-raster bonds, and may also exacerbate shrinkage and warpage issues (Section 2.2.1).

Another major obstacle is the high melt viscosity of HPPs [36] (Section 2.2.2). Dealing with viscous materials is particularly challenging in FFF due to the design of the print head, which leads to a very short travel distance within the liquefier where the polymer filament is heated and melted. The torque required to push the molten material out puts significant stress on the feeders, resulting in substantial wear and tear on the extruder head [37].

Another problem frequently observed in FFF that is worsened with HPPs is the distortion of the printed part occurring as the polymer cools down on the build plate [38,11,23] (Section 2.2.3). This means that large HPP parts cannot take full advantage of the geometric freedom afforded by FFF, as they are more sensitive to differential cooling and hence to shrinkage- and crystallisation-related distortion.

Lastly, many HPPs are hygroscopic [39]. Moisture absorption can produce swelling at the macroscale, and water molecules can interfere with inter-molecular chain bonds, which changes the processability and mechanical properties of the printed part [40] (Section 2.2.4).

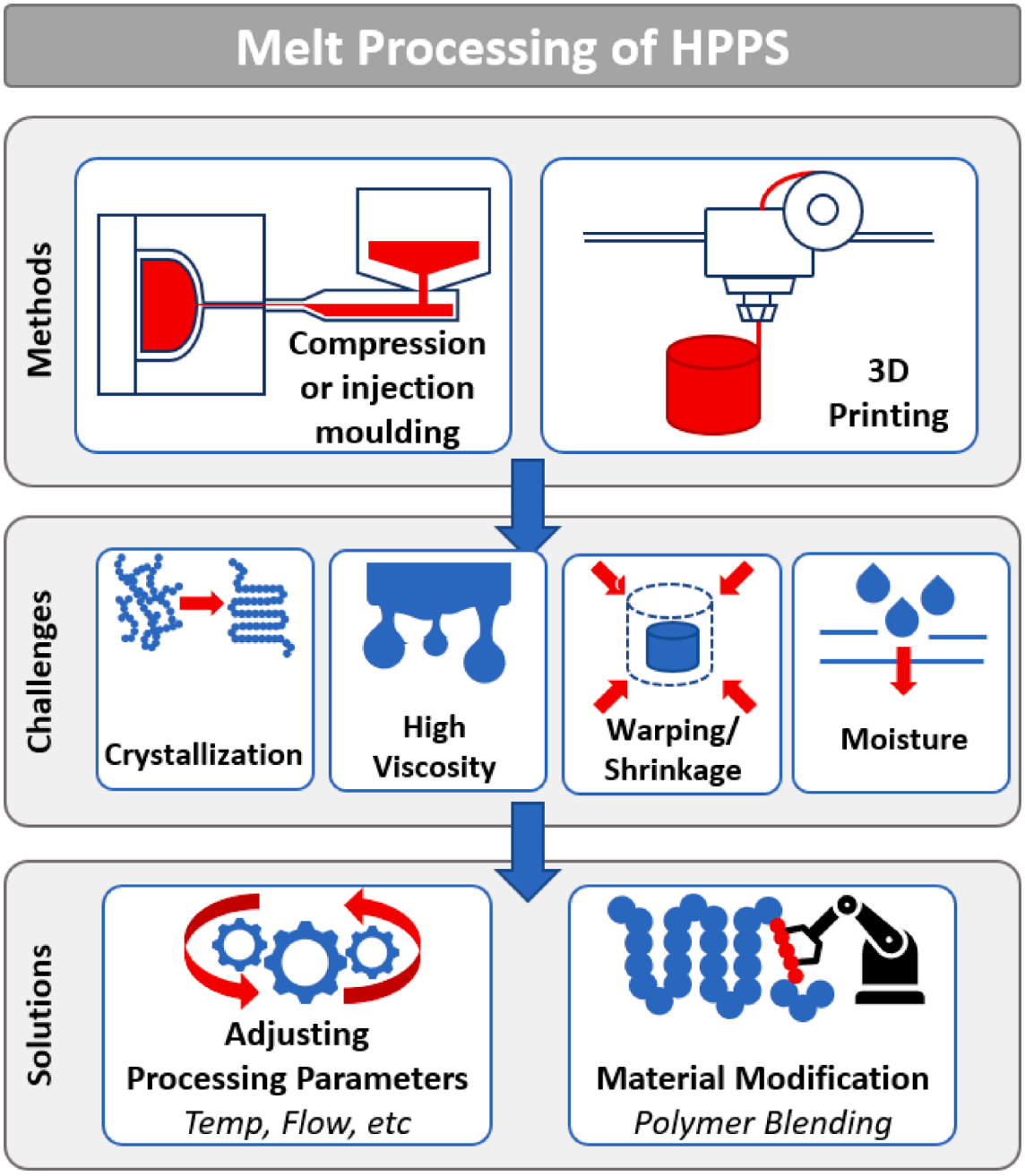

Fig. 3. Graphic summary of the material-related issues arising in melt processing of HPPs and the two main ways of alleviating them, i.e., adjustment of the processing parameters and modification of the material itself, in this case, via polymer blending as opposed to redesign of the chemical structure of HPPs.

2.2.1. Crystallinity

Feedstock materials for FFF can be generally divided into semi-crystalline or amorphous thermoplastics (Fig. 4). Amorphous polymers only contain disordered chains. Conversely, semi-crystalline polymers are able to arrange themselves into ordered (crystalline) structures by 'folding' their polymeric chains. This results in several differences [41]. Firstly, amorphous polymers do not have a defined Tm; rather, they soften over a range of temperatures that is conventionally defined through the Tg. Semi-crystalline polymers have both a Tg and a Tm, as crystalline structures require additional heat for melting [42].

A large proportion of HPPs are semi-crystalline. As a matter of fact, crystalline structures are able to establish stronger intermolecular bonding and can tolerate greater stress loads [43]. Some conventional polymers commonly used in FFF are also semi-crystalline. This is the case, for example, of PLA and polyamide (PA, aka nylon). However, printing semi-crystalline HPPs is more challenging due to their tendency to crystallize more rapidly [41]. In this regard, though, it should be mentioned that the crystallization rate may be different among different HPPs. For a given polymer, the crystallization rate is also affected by the molecular weight, as high molecular weight semi-crystalline grades take longer to crystallise than their low molecular weight variants, and by the complexity of the molecular structure, as observed, for example, for different isomers of the same polymer [44].

Another important consideration is that, for semi-crystalline polymers having fast crystallization kinetics, the rate of crystallization significantly affects inter-raster and inter-layer bonding [45]. In fact, crystallization inhibits the movement of polymer chains across the interface between neighbouring strands and subsequent layers. Crystal structures act as pinning points that prevent the diffusion of polymer chains, leading to weak inter-strand bonding and subsequently to inferior mechanical strength in the printed part compared with the bulk polymer [46].

During printing, thermal gradients arise between the freshly deposited material, which is still hot, and the previously deposited strands and layers, which are at a much lower temperature, and these gradients are built into the printed part. This is particularly problematic when printing larger parts where the nozzle must travel to greater distances between layers. As a result, there may be differences in the crystallinity at each layer of the printed part, or even within the same layer, resulting in locally heterogeneous values of toughness and other mechanical properties [11]. Upon crystallization, the polymer chains form ordered structures, quickly resulting in volumetric contractions that can also worsen shrinkage/warping phenomena [47].

2.2.2. Viscosity

When shear is applied to a molten polymer, molecular chains drag against one another due to intermolecular attraction, and this results in viscosity. The melt viscosity of a polymer plays a critical role in FFF, as it governs the flow through the nozzle and the deposition on the base platform or previous layers [15,47]. To be printable, thermoplastic materials for FFF are typically non-Newtonian and shear thinning in the molten state. At a given temperature, shear thinning fluids experience a change in viscosity (η) due to a change in shear rate ($\dot{\gamma}$) according to the Ostwald-de Waele power law fluid model, which can be expressed as [48]:

$$\eta(\dot{\gamma}) = \varphi \bullet \dot{\gamma}^{n-1} \quad (1)$$

where φ is the flow consistency index, and n is the power law index. The shear rate, in its turn, depends on the printing conditions and especially on the flow rate (Q) [49].

Printing high viscosity polymers like HPPs by FFF is very challenging because the molten filament must be forced to flow through a very small nozzle, which generates a strong backpressure. If the melt viscosity becomes too high, the printer is likely to clog due to excessive back-pressure causing the filament to buckle [50,51]. Also, the high viscosity often produces grinding of the filament and poor interlayer adhesion due to the lack of flowability of the polymer [52]. Conversely, if the melt viscosity becomes too low, flow inconsistences and loss of shape are likely to occur, as demonstrated, for example, in the study by Geng et al. [53]. Another issue which may arise if the melt viscosity becomes too low upon printing is backflow, whereby the molten material flows back

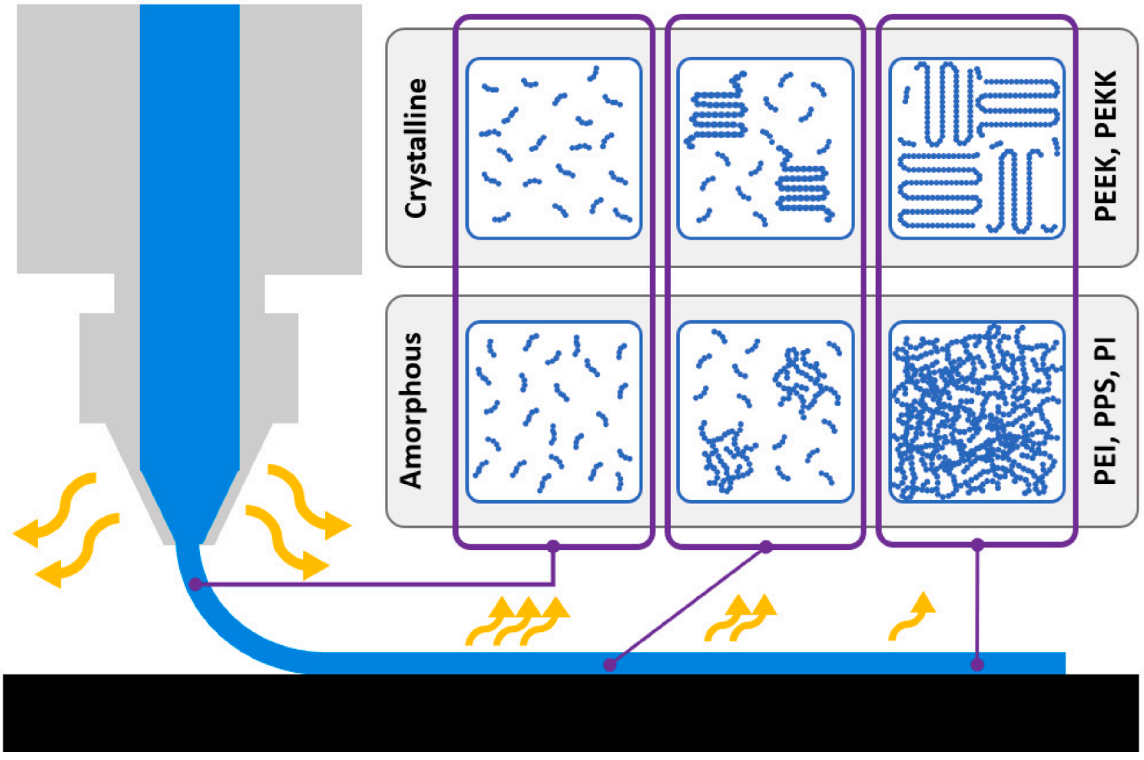

Fig. 4. Schematic showing the different structural behaviour of amorphous and semi-crystalline polymers upon cooling.

up along the liquefier column of the hot end [48].

The rheological behaviour in the molten state also affects the extrusion of the feedstock filament itself, as it governs the ability of the filament to retain the targeted diameter at the exit of the spinneret. Dimensional stability of the filament is crucial since inconsistent diameter of the filament will result in under-extrusion, clogging of the nozzle and poor-quality printed parts [52].

A careful balance is thus needed to ensure the viscosity is within a range suitable for even extrusion and high printed part quality. For a given polymer, viscosity is directly proportional to the average molecular weight, and is also influenced by the molecular weight distribution [36,54]. Moreover, polymer chains with stronger intermolecular attraction have greater drag forces and result in greater viscosity, as seen in HPPs [55,56].

As mentioned before, the melt viscosity depends on the processing conditions, especially the shear rate and temperature, where an increase in temperature generally reduces the melt viscosity. Ajinjeru et al. [57] analysed the rheological behaviour of HPPs to identify successful extrusion settings. Meanwhile, several studies have attempted to mitigate viscosity-related issues through a special redesign of the hot end [58]. While very effective, the redesign of the printing equipment may be difficult to translate from research to industrial practice, which calls for different strategies that allow HPPs to be easily managed on existing commercial printers.

2.2.3. Shrinkage/warping

Shrinkage of 3D printed parts is a common issue amongst commercial polymers like ABS and is frequently noted also with HPPs [59]. The non-uniform chamber temperatures result in uneven thermal distribution and subsequent dimensional instabilities and warping once the part is cooled to room temperature [59]. Volumetric changes are particularly problematic if the printed part is large and features a complicated geometry [60].

Shrinkage and warpage are strongly influenced by the coefficient of thermal expansion (CTE) of the polymer [52]. In thermoplastic polymers, a change in CTE is associated with the glass transition. For instance, the CTE of PEEK significantly varies whether the material is above (5.5×10^{-5} K^{-1}) or below (14.0×10^{-5} K^{-1}) its Tg (143 °C). Preventing significant dimensional instability by keeping the CTE in the range above Tg during the printing process will assist in producing a high-quality HPP part [61]. If the polymer is semi-crystalline, its rate of crystallization is also very important [41]. Besides the intrinsic properties of the polymer, it is known that a discontinuous flow through the nozzle due to inconsistent filament diameter may encourage uneven cooling in the printed part and result in warping [62].

Some common ways to minimise shrinkage and warpage issues harness the thermal behaviour of polymers. For example, increasing the printing temperature of high-density polyethylene (HPDE) composites from 200 to 260 °C reduced warping due to the longer time being available for the polymer chains to reach their relaxation time (or time taken for diffusion to occur), thus preventing thermal stresses from being locked into the part [63]. Through the careful control of temperature, C. Yang et al. [64] were able to manipulate the level of crystallinity within the printed part, which remediated the volumetric contraction due to shrinkage. Heating the build chamber can also be very helpful [16]. For example, Wu et al. [65] observed that increasing the chamber temperature during the printing of PEEK parts mitigated warpage associated with uneven cooling. Increasing the bed temperature has also been shown to reduce shrinkage and warpage by reducing thermal stresses [66]. Specifically, the bed plate temperature must be carefully selected to ensure the material stays above its Tg while printing. However, increasing the bed plate temperature too much may result in delamination due to steep thermal gradients [67].

Shrinkage and warpage can also be tackled by optimising the g-code [68] or implementing a post-processing heat treatment like annealing to release thermal stresses [69]. Léonard and Tammas-Williams [70] proposed that using bespoke auxiliary internal structures, rather than the default AM software-generated infill, reduces shrinkage, particularly if circular objects are to be printed.

Otherwise, in terms of printing hardware, Hu et al. [71] demonstrated that temperature uniformity around the print nozzle can be improved by redesigning the hot end to include a heat collector (HC) module. Despite its effectiveness, implementing this option may be time consuming and not applicable for all research.

2.2.4. Sensitivity to moisture absorption

Moisture absorption deeply affects the final quality of the printed part [72]. The rate that moisture enters a polymer depends on the polymer's properties, especially its water diffusivity. Moisture uptake is also affected by the object's geometry. Intuitively, moisture absorption is more prevalent at the edges and surfaces of an object, whereas the interior requires more time to reach an equilibrium [73]. Quite often, water absorption in printed parts has been shown to obey Fickian diffusion laws regardless of temperature [74]. For instance, ULTEM 9085 (which is a commercial PEI-polycarbonate (PC) blend) is known to follow Fickian-type moisture diffusion [39]. While water uptake has a plasticising effect that may lower the molten viscosity of ULTEM 9085 and strengthen interlayer bonding, moisture absorption above 0.1 wt% results in a significant decrease in ultimate tensile strength, because water molecules interfere with the hydrogen bonds between polymer chains [75]. Although the Fickian behaviour is very common in FFF parts, exceptions exist, especially if the feedstock is a composite material. For example, it has been observed that, if PLA is blended with bamboo fibres, the filler preferentially absorbs water, and this impedes the establishment of normal Fickian diffusion [76].

If the polymer is semi-crystalline, quite often, water is first absorbed into the amorphous regions, where it acts as a plasticiser, reducing the Tg and increasing the chain mobility. Subsequently, water molecules can also penetrate the crystalline phase and lower the degree of crystallinity [40]. Certain polymers like nylon and PC are heavily hygroscopic, which is due to the polarity of their chemical structure that attracts water molecules [77,78]. In contrast, other semi-crystalline polymers like PLA have chemical structures that are hydrophobic, and hence less prone to moisture uptake. Nonetheless, PLA can still be degraded when water molecules break the ester bonds [79].

The effect of moisture absorption on thermoplastic filaments before printing is complicated. For example, Wichniarek et al. [80] found that moist filaments with maximum moisture absorption of 0.6% can still be printed. Other studies have shown that moisture absorption increases the diameter of amorphous filaments by a maximum of 0.03 mm and is not directly responsible for nozzle clogging, but rather water molecules reduce the Tg leading to changes in viscosity and flow properties of the polymer [81].

3. High-performance polymers in FFF

HPPs, as defined by Hergenrother [14], are polymers recognized for their superior mechanical properties including, but not limited to, tensile strength, hardness, dimensional stability and toughness. These properties are not affected when exposed to high temperatures or harsh chemical environments, which is a peculiarity of HPPs. The exact criteria for a polymer to be defined as HPP can be summarised as follows [14]:

- The material must be able to retain structural integrity when exposed to 177 °C for more than 10,000 h while subjected to short or long-term mechanical, electrical and chemical stresses.
- While under 1.52 MPa load, the material should deflect by no more than 10% at a temperature of 177 °C or above.
- The minimum thermal decomposition point (corresponding to 5% mass loss) of the material should be no less than 450 °C.

The key difference between HPPs and engineering/commodity polymers is the chemical makeup of their polymeric structures that imparts higher resistance to thermal and mechanical stresses. As seen in Fig. 5, the mechanical strength and thermal stability of HPPs primarily come from the presence in their molecular structure of numerous aromatic (and, sometimes, heterocyclic) rings, whose carbon–carbon bonds have a dissociation energy much higher than common carbon–carbon single bonds [14]. Another important aspect of the chemical structure of HPPs is the ability to establish secondary inter-molecular bonds (i.e., hydrogen bonds, van de Waals forces and polar interactions), which deeply affect properties like the Tg or Tm.

As previously mentioned, the molecular structure and inter-molecular interactions that are responsible for the strength and stability of HPPs are also responsible for the difficulties in melt processing, including by FFF. A possible way to introduce flexibility into the polymer chain backbone and to reduce intermolecular interaction forces (measured as a reduction in Tg) consists in modifying the chemical structure of the polymer. Notable methods include [82]:

- Encouraging asymmetry of the chemical structure
- Introducing specific chemical bonds with a high rotational degree of freedom (i.e., -O- or -S-)
- Adding bulky side groups like $-CF_3$ or $–CH_3$

All these methods serve to interfere with the formation of strong intermolecular bonds between the chains, preventing them from heavily packing together [83,84]. Using these methods will reduce the complexity of printing HPPs by lowering their processing temperature and their melt viscosity [83]. However, chemical modification may be unpractical or uneconomical, because it is expensive and time consuming to produce polymers in large enough amounts with specific chemical structures for printing.

Another important factor is the molecular weight distribution of the polymer. Longer polymer chains are more difficult to separate upon heating due to increased entanglement and stronger intermolecular interaction from secondary bonding forces. Conversely, short polymer chains are not so strongly linked, and therefore have lower processing temperatures. However, they also have weaker mechanical properties [36,85].

HPPs tend to have high molecular weight, which contributes to their exceptional thermal stability and mechanical strength. However, this

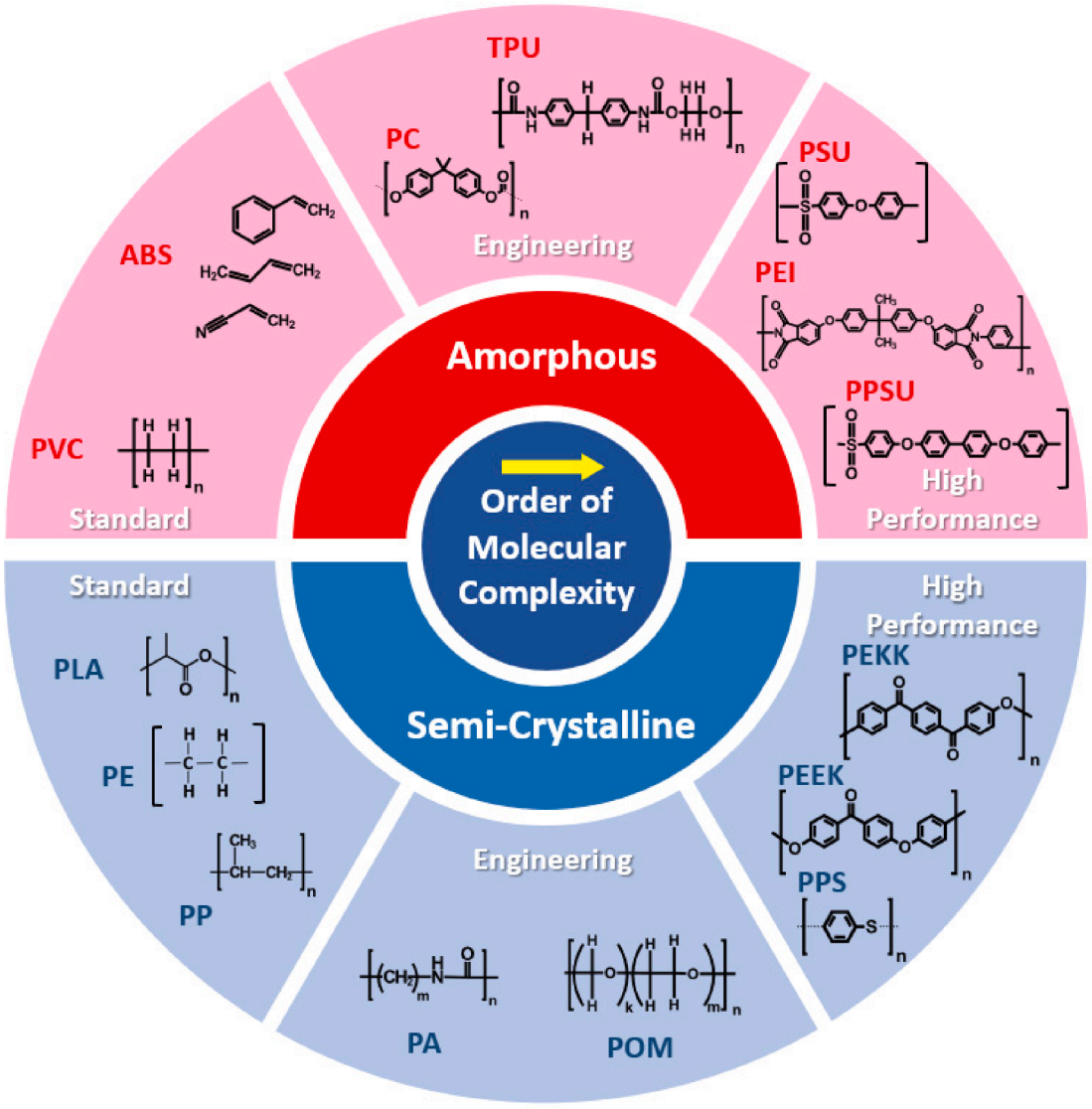

Fig. 5. Schematic showing the increasing complexity of the chemical structure obeserved (from left to right) in standard, engineering, and high performance polymers used in FFF.

makes them also difficult to process under melt conditions. To improve the melt processability of HPPs, the average molecular weight and distribution can be modified to include low molecular weight polymer chains acting as plasticisers and reducing the melt viscosity [86]. This polymer blending technique has already been utilized in several melt processing techniques [87], demonstrating reduced viscosity of the polymer melt and hence mitigated thermal requirements from the processing equipment. These short polymer chains are also well known to improve the interlayer strength of FFF printed parts, resulting in higher mechanical strength and reduced anisotropy [32].

4. Current state of the art in the FFF of HPPs

Despite the printing difficulties, HPPs in AM have been used in a variety of applications as shown in Fig. 6. Some of these applications include high temperature gas/oil separation plants [88], biomedical implants [89], anti-corrosion systems [90], dentistry [91], prosthetics [92], membranes [93], radiation containment [94], energy absorption [95], fuel efficiency improvement [96], tough coatings for nuclear reactors [96], electrical insulation [97] and microelectronics [98]. The following sections present and discuss the state of the art in the FFF of HPPs.

4.1. Poly-ether-ether-ketone (PEEK)

PEEK is a popular HPP for 3D printing due to its excellent mechanical properties and high thermal resistance with a Tm of approximately 350 °C. PEEK also has exceptional wear resistance, chemical stability, and resistance to ultraviolet radiation [99], making it highly suitable for aerospace applications such as the fabrication of nanosatellites [100]. For similar reasons, PEEK has widespread use in the biomedical industry for biomedical devices [61], oral implants [101] and orthopaedic applications [102]. PEEK has also been utilised in the production of negative Poisson's ratio metamaterials [103].

The review by Zanjanijam et al. [8] summarizes the optimum printing conditions for PEEK. While searching for the best printing parameters leading to defect-free PEEK parts, Zanjanijam et al. [8] acknowledge that printing by FFF exacerbates several issues commonly observed with other melt processing technologies like injection moulding, including warping, poor dimensional accuracy, and subpar mechanical properties. A recent study by Vidakis et al. [104] found that layer height was an important parameter that, when set at 0.1 mm, made

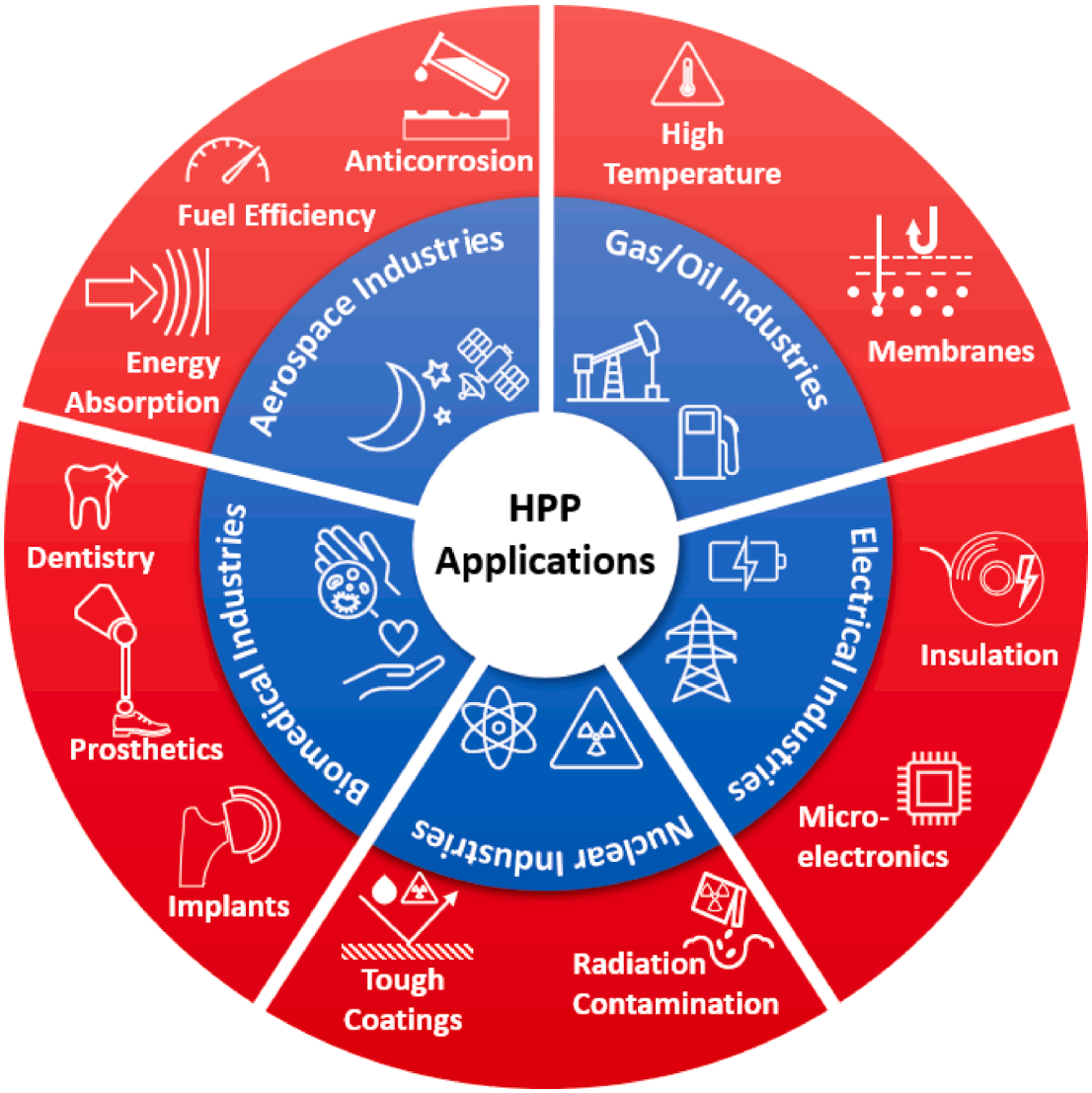

Fig. 6. Applications of additively manufactured HPPs, including high temperature gas/oil separation applications [88], biomedical implants [89], anti-corrosion applications [90], dentistry [91], prosthetics [92], membranes [93], radiation containment [94], energy absorption [95], improving fuel efficiency [96], tough coatings for nuclear applications [96], electrical insulation [97] and microelectronics [98].

it possible to maximise the tensile strength of the printed samples, although this was at the expense of a longer printing time and more energy being required to complete the print. Generally, high bed and chamber temperatures are preferable for producing PEEK parts having high tensile strength, because increasing the temperature upon printing reduces the melt viscosity of the polymer and promotes interlayer bonding [68]. Interlayer bonding can also be encouraged with a chemical redesign of PEEK, for example through the addition of 10 mol.% of fluorene groups to the PEEK chain [45]. Also, a common method to improve the stiffness and strength of PEEK is to combine it with either short [105,106] or continuous carbon fibres [107]. However, functionalising PEEK with short carbon fibres may increase the melt viscosity and ultimately result in voids and poor interlayer bonding [105].

A major problem with FFF of PEEK is the rapid crystallization that occurs during printing. Coupled with the temperature fluctuations within the 3D printer, the fast crystallization of PEEK means that the part produced will have various levels of crystallinity, as often revealed by colour variations across the part [65]. As previously mentioned, (Section 2.2.3), crystallization can lead to warping and affect the dimensional accuracy of the part. Whilst some of these issues can be alleviated with post-printing annealing [108], shrinkage remains a major issue with PEEK. According to some authors, PEEK must be printed at temperatures below 380 °C, since above this temperature shrinkage proceeds at a faster rate than inter-strand diffusion does, which undermines consolidation [38]. However, He et al. [109] were able to print PEEK at 440 °C and achieve excellent mechanical strength. Although the authors did not comment on warping or shrinkage, the samples were annealed, which likely helped remediate this issue, if needed [109]. Predictive models have been developed and machine learning capabilities grown to estimate where warping will occur considering material's properties, part's geometry, and thermal environment. However, most of these are early-stage models still requiring more research before they can be applied to any PEEK printed part for industrial applications [110].

4.2. Poly-ether-ketone-ketone (PEKK)

The literature regarding the use of PEKK in FFF is still relatively limited compared to PEEK. In terms of chemical structure, PEKK differs from PEEK because it has an additional ketone group. This results in different thermal and viscoelastic behaviours, with relevant consequences for FFF [111]. One difference is that, due to the additional ketone group, PEKK can generate the same crystalline structures as PEEK plus another crystalline form (orthorhombic structure, a = 0.393 nm, b = 0.575 nm and c = 1.016 nm) which can be induced by exposing quenched non-crystalline films to methylene chloride (solvent crystallization) [112].

By varying the chemical structure of PEKK (specifically the para/meta phenyl isomer ratio), its properties can be intrinsically modified in terms of thermal behaviour, viscosity, and crystallisation kinetics [113]. PEKK also has a lower crystallization rate than PEEK (by about 3 orders of magnitude) which may suggest a reduced tendency to warping, although this has not been explicitly proven [114]. This slower crystallisation certainly improves interlayer bonding since PEKK remains in an amorphous state for longer than PEEK, and this gives more time for interlayer diffusion to occur [115]. This may facilitate FFF printing of PEKK over other HPPs and has led to the commercialisation of a PEKK filament by Stratasys [116]. PEKK has also been employed to successfully print parts for Boeing's CST Starliner, a space taxi used for transport between earth and the ISS [117]. The versatility of PEKK in FFF is further proved by the successful fabrication of biomedical parts, including implantable devices that leverage the biocompatibility of PEKK [118]. Fillers can provide PEKK with added functionality, as shown, for example, by carbon nanotube filled PEKK [119] being proposed for electrostatic discharge applications in space to prevent surface charge build-up that could damage equipment.

Several papers by Rashed et al. [10,120] have explored the effect of various printing parameters on the mechanical properties of PEKK. Lepoivre et al. [121] found that the dependence of PEKK's surface tension on temperature strongly impacted the extent of interlayer bonding. The study suggested that the difference between the chamber temperature and the temperature of the deposited material was more influential on polymer healing and sintering than the extrusion temperature itself [121].

PEKK may also suffer from shrinkage upon cooling. However, as shown in the study by Kennedy et al. [122], adding fillers like mica may improve the dimensional stability of PEKK. As the authors stated, other fillers like carbon nanotubes could also deliver the same effect.

4.3. Polyphenyl sulfide (PPS)

Like PEEK and PEKK, PPS is a semi-crystalline HPP that offers excellent chemical resistance and stability at high temperature (continuous use temperature of 220 °C), in spite of having a relatively low Tg (85 °C) with a Tm of 285 °C [123]. PPS is transparent, has exceptional hydrolytic resistance, and shows high dimensional stability when compression or injection moulded [124]. Garmabi et al. [125] proved the suitability of FFF-printed PPS for the production of a coolant inlet tube in the automotive industry. Martinez et al. [126] mixed PPS with carbonyl iron particles and demonstrated that the PPS-based composites were more suitable for microwave absorber applications than the PLA-based counterparts. Thanks to the addition of thermotropic liquid crystalline polymer (TLCP) fibres, the tensile strength of PPS parts increased from 45 MPa to 60 MPa [127]. With values greater than 2 GPa, the tensile strength of carbon fibre-reinforced PPS may exceed the strength of some aerospace metals like aluminium and some titanium alloys [128].

Retolaza et al. [129] found that increasing layer height and infill degree may enhance the tensile strength of PPS parts. Meanwhile, the authors cautioned that increasing the volumetric flow may adversely affect warping and dimensional stability. Additionally, optimising the g-code parameters has been shown to improve the tensile strength of PPS samples to reach nearly the same strength as compression moulded samples [125]. According to El Magri et al. [130], annealing the printed samples for 1 h at 200 °C can significantly improve dimensional stability whilst increasing the level of crystallinity. As a result, thermally annealed PPS parts exhibit higher Tg and higher tensile strength values than as-printed samples. This was also verified by other studies showing that interlayer bonding in PPS samples can be enhanced with appropriate post-printing heat treatments [131,132].

4.4. Poly-ether-imide (PEI)

In contrast to the above mentioned HPPs, PEI is a fully amorphous HPP. PEI boasts an excellent strength-to-weight ratio and high flame-retardant capacity, which makes it an outstanding candidate for aerospace applications. Printed PEI has been successfully used in zero gravity environments like aboard the ISS [9]. Another application for PEI is in the biomedical field. Porous PEI scaffolds may be ideal for bone defect repair since the Young's modulus of the printed scaffolds can be tuned to match the properties of human bone tissue [133]. Printed PEI parts reinforced with carbon fibres and carbon beads have been evaluated for their suitability in small wind and tidal turbines owing to their low deformation and minimal mechanical deflection [134].

Stratasys currently commercialises two different PEI-based filaments for FFF, namely ULTEM 1010 [135], which only contains PEI, and ULTEM 9085, which is a blend of PEI/PC [136] (discussed in more detail in section 6.3.1). Several optimization studies have been conducted to define the best printing parameters for ULTEM 1010. However, conflicting conclusions can be found in the literature due to the different g-codes being used to manufacture the samples. For instance, Gebisa and Lemu [137] found that only the raster angle significantly affects the

tensile properties of the printed parts, whereas Ouassil et al. [138] reported that the print speed was the most impacting factor on the density and the tensile properties of the printed samples.

Annealing at 225 °C for three hours has been suggested as an effective strategy for improving the tensile strength of printed ULTEM 1010 from 66.5 to 75.1 MPa [139]. Han et al. [140141] used a laser to locally provide additional heat while printing and promote interlayer bonding in order to increase the isotropy and tensile strength in ULTEM 1010 printed samples. Wu et al. [142] printed flame-retardant parts made of ULTEM 1010 mixed with hollow glass microspheres, nanoclay, and non-halogenated flame-retardant additives. Incorporating 0.6 wt% of carbon nanotubes in PEI has been shown to improve interlayer bonding in FFF parts and stabilise the part's geometry upon annealing [143]. The presence of carbon nanotubes can also be useful for the fabrication of piezoresistive sensors [144].

4.5. Thermoplastic polyimide (TPI)

Further to PEI, the family of polyimides (PIs) includes other polymers of interest for FFF. Whilst PIs normally exist as thermosets, these polymers can also be thermoplastic, in which case they can be classified as a semi-crystalline HPP [145]. Abbot et al. [146] explored some of the specific challenges that arise when the thermosetting variant of PI is adopted in solution-based 3D printing processes. However, when it comes to melt extrusion (FFF printing), the thermoplastic form (TPI) is strictly required. TPI has a very high impact strength and corrosion resistance. Thanks to its thermal stability, TPI can remain in operation up to 240 °C [147]. In spite of these advantages, studies into FFF printing of TPI are still very limited. Wu et al. [148] discovered that the narrow printing range of TPI has important implications for the print quality and interlayer strength of the samples. Specifically, printing above 320 °C was required to turn TPI from an elastic state to a viscous flow state, but increasing the temperatures above 340 °C caused the material to foam [148]. Moisture absorption in the TPI filament was found to be an important factor increasing the porosity and reducing the tensile strength of the printed samples [149].

4.6. Polysulfones

Polysulfones are a class of HPPs characterized by an aryl-SO_2-aryl subunit. They can be divided into polysulfone of bisphenol A (PSU), polyether sulfone (PES), and polyphenylene sulfone (PPSU) [150]. Polysulfones are amorphous polymers with a very high processing temperature compared with other melt-processable thermoplastics. Several aromatic rings in the chemical structure of polysulfones provide high strength and stiffness [151].

As of the time of publishing this review, to the best of the authors' knowledge, there were no studies in the literature related to the FFF printing of PES or PSU.

PPSU has been utilized in the production of dental prostheses as a replacement to PEEK [152]. The study by Schönhoff et al. [154] claimed that the flexural strength of PPSU was comparable to PEEK, however the mechanical response was not tested on 3D printed samples, but rather on compression moulded bars. As for the printed samples of PPSU, the flexural strength ranged between 75 and 80 N/mm^2. In a recent study [153], when PEEK was replaced with PPSU in a test to determine the tensile bond strength between the polymer and a veneering composite resin, it was found that the tensile bond strengths were comparable. However, since PEEK was not 3D printed, the results are difficult to interpret, because the manufacturing method was different for the two polymers. The addition of carbon fibres to PPSU was shown to increase its viscosity threefold. However, the PPSU-carbon fibre composite was not printed, but only evaluated for its suitability as a potential feedstock for large scale AM [154]. Ultimately, there is still little understanding on where the mechanical properties of PPSU lie, and it is premature to benchmark them against the mechanical performance of parts printed with other HPPs.

5. Polymer blending

Clearly, in spite of the increasing success of FFF printing of HPPs, major challenges remain due to the high printing temperatures required, the high melt viscosity, the strong propensity for shrinkage and warpage, and the likely absorption of ambient humidity. A convenient way around this consists in blending HPPs with other selected thermoplastics.

Comparable to metal alloys, polymer blends are obtained from the combination of at least two polymers to produce a material with new physical properties. Sectors like the food packing industry frequently use polymer blending techniques to improve processability, increase material properties like chemical resistance and mechanical strength, and quickly respond to market changes and requests for new materials [155].

The microstructure and properties of polymer blends are highly dependent on the compatibility between the polymers (refer to Fig. 7). This results in three broad categories of polymer blends [156]:

- ***Homogenous/Miscible blend*** – after blending, the constituents exist in a single phase, resulting in a single Tg. Miscible blends are most commonly observed when the polymers have similar chemical structures.
- ***Heterogenous/Immiscible blend*** – after blending, the constituents exist as separate phases, resulting in distinct Tg values.
- ***Compatible polymer blend*** – an immiscible polymer blend with strong interactions between the constituents, resulting in macroscopically uniform properties.

If an immiscible blend is considered, material properties like the mechanical strength of the blend are highly dependent on the interaction between the blended phases. Due to the poor thermodynamic phase stability, immiscible polymer blends experience a strong propensity to phase separation, whereby the less abundant polymer phase forms coarse domains within the more abundant polymer matrix. The interfacial adhesion between immiscible polymers is generally weak, and this undermines the mechanical properties of the blend [157]. Microstructural manipulation is thus necessary to improve the mechanical strength of immiscible polymer blends, which can be achieved either by reducing the coarseness of the microstructure (i.e., reducing the size of the polymer dispersion) or by increasing the adhesion between the polymer phases.

interfacial adhesion can be enhanced through compatibilization strategies that promote the formation of chemical or physical bonds between the polymer phases [158]. This can be done either through nonreactive compatibilization or through reactive compatibilization. Nonreactive compatibilization uses graft or block co-polymers that contain segments that are compatible with both phases. The copolymers have the tendency to migrate and localise in the interfacial region between the polymer phases. The different segments of the copolymers orient themselves towards the phase they are compatible with, and, working like a bridge, bring stability to the polymer blend [159]. Reactive compatibilization is the process by which block or graft copolymers are generated *in situ* directly within the interface regions of the immiscible polymer phases, where they compatibilize the blend and limit the coalescence of the dispersed polymer domains, thus reducing the coarseness of the microstructure [159].

Blending may have complicated consequences on the properties of semi-crystalline polymers, including phase morphology, crystallization rate, and nucleation processes. In this respect, it is important to distinguish between miscible and immiscible blends, and then between blends that contain semi-crystalline/amorphous polymers and blends that only contain semi-crystalline polymers. In miscible polymer blends, when a semi-crystalline polymer begins to crystallize, the composition of the

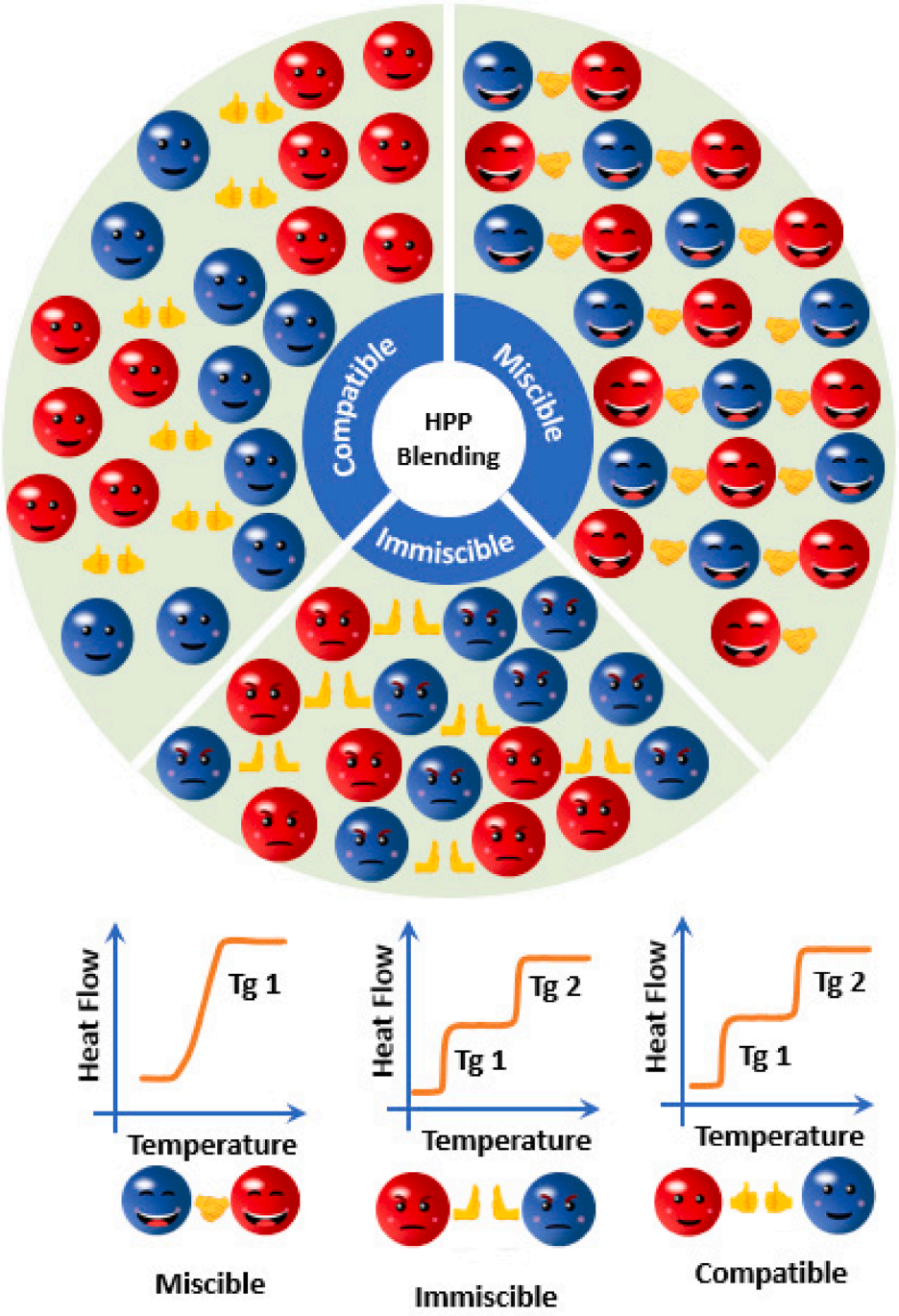

Fig. 7. Different types of polymer blends leading to differences in thermal behaviour, especially Tg.

residual amorphous phase diverges from the nominal blend composition. Meanwhile, the presence of another polymer within the amorphous phase of the blend changes the thermodynamic conditions and may result in a change in crystal growth kinetics for the semi-crystalline polymer [160]. When both polymers in the blend are semi-crystalline, co-crystallization may occur if the molecular structures of the polymers are isomorphous. Otherwise, concurrent crystallization may happen if crystallization of the miscible polymer phases occurs in the same temperature region [160].

In immiscible polymer blends, if the blend contains a large proportion of an amorphous phase and a minor fraction of a semi-crystalline polymer, the amorphous phase significantly affects the growth of the crystalline phase due to volumetric constraints. In other words, the amorphous matrix impairs the polymer chain mobility in the dispersed phase domains and inhibits crystal growth. In immiscible blends where both polymer phases are semi-crystalline there is little to no interaction between the phases [160].

6. HPP-based blends

Blending HPPs with other HPPs or with commodity and engineering polymers can improve existing properties of the individual polymers or even impart new functionality (refer to Fig. 8), like lowering the melt viscosity or the printing temperature to facilitate processing, interfering with the advancement of crystallization to reduce warping/deformation, or improving the desired mechanical properties like tensile strength,

Fig. 8. Summary of HPP-based blends relevant to FFF.

toughness, or wear resistance. Numerous examples of HPP blends are critically reviewed in the following sections, with an emphasis on the HPPs that are most often employed in FFF like PEEK, PEKK, PEI and PPS. Likewise, particular attention is paid to the effects of blending (e.g., lowering the melt viscosity, controlling the crystallisation, reducing the moisture adsorption) that are expected to ease the 3D printing of HPPs and to provide FFF parts with improved mechanical strength or new embedded functionality.

6.1. PEEK-based blends

6.1.1. PEEK/polysulfones

Great attention has been paid in the literature to PEEK-based blends containing either PSU or PES. PEEK and PSU produce immiscible blends [161]. In terms of mechanical strength, PEEK/PSU blends do not always have a higher mechanical strength compared with neat PEEK. However, it is advantageous to add PSU (20 wt%) to PEEK since the mechanical strength of the blend is close to that of neat PEEK, whilst the presence of PSU reduces the viscosity and eases the melt processability of PEEK [162]. Hoffman et al. [163] found that, if PEEK/PSU (70/30 wt%) blends were compatibilized with segmented PEEK/PSU block copolymers and reactive end-functionalized PEEK and PSU oligomers, the size of the PSU domains dispersed in the PEEK matrix could be sensibly reduced. In samples containing 0.5 and 1 wt% of oligomer mixture, the notched impact strength increased from approximately 70 to 95 kJ/m^2 relative to the non-compatibilized blends.

Although PEEK and PES are generally considered immiscible through melt blending, Malik [164] demonstrated that PEEK and PES may have some miscibility thanks to the interaction between the polarizable sulfonate structure in PES and the carbonyl side chain in PEEK. In particular, increased compatibility was observed in PEEK-rich compositions compared with PES-rich ones, as PEEK dissolves into PES to a greater extent than the opposite [165]. Although PEEK and PES are not normally miscible under melt processing conditions, they can become miscible under other processing techniques like solution casting [166,167]. Alternatively, the two polymers can be dissolved into concentrated sulfuric acid and precipitated into a PEEK/PES blend [168].

The addition of PES to PEEK offers several advantages in light of FFF printing. PES has lower viscosity compared with PEEK, and when blended in any proportion into PEEK, produces a blend with reduced viscosity compared with neat PEEK [169]. The polymer chains of PES

also hinder the crystallization of PEEK [164]. However, due to the limited miscibility, PEEK/PES blends may have poor mechanical properties and, despite the sulfonate-carbonyl interaction, a compatibilizer is required to further promote compatibility between PEEK and PES in melt processing techniques. Partial miscibility can be encouraged by melt blending at 375 °C and combining the polymers with phenolphthalein. This is a chemical that acts as a compatibilizer between PEEK and PES, and also acts as a plasticizer for PES [170]. A variation of PEEK, polyetheretherketoneketone (PEEKK) can also be blended with PES, and the compatibility can be increased with the addition of PEEK oligomers. The PEEKK-PES-PEEK ternary blend produces a partially compatible system with low concentrations of PES [171].

Post processing methods can also improve the mechanical performance of PEEK/PES blends. For example, Arzak, Eguiazábal and Nazába [172] found that annealing PEEK/PES injection moulded samples at 185 °C for 24 h remarkably increased the tensile yield stress when compared to the unannealed PEEK/PES samples, irrespective of the blend composition. To illustrate, the yield stress ranged (indicatively, based on graphical data) between 74 and 81 MPa for the as-moulded samples, and between 93 and 96 MPa for the annealed samples. However, the impact strength decreased, especially for HPP blends rich in PES. For the 50:50 composition, the impact strength decreased (indicatively) from 82 to 50 J/m after annealing. This was primarily attributed to the increase in crystallinity of the PEEK phase, although further investigation was suggested to understand the effect of annealing on the interfacial region between the phases.

Alternatively, fillers can be added to enhance the mechanical strength of PEEK/PES blends. Mandal and Alam [173] discovered that a 75:25 (wt:wt) PEEK/PES blend functionalised with 0.84 vol% of barium titanate ($BaTiO_3$) had higher overall mechanical properties compared with the neat polymer blend, including higher tensile strength (increased by 13%) and higher tensile modulus (increased by 5.2%).

6.1.2. PEEK/PEI

PEI is totally miscible in amorphous PEEK regardless of the composition of the blend [174]. However, when PEEK crystallises, PEI is rejected into the amorphous regions. As the crystallisation of PEEK proceeds, the amorphous phase becomes progressively richer in PEI. Since the Tg of PEI is much higher (by 75 °C) than the Tg of PEEK, the enrichment in PEI leads to a progressive increase of the Tg of the amorphous domains. Ultimately, if the Tg exceeds the crystallisation temperature of PEEK, crystallisation will cease due to vitrification of the amorphous domains [175]. The addition of increasing PEI content to PEEK can also aid in reducing the viscosity of the blend [176], which can significantly improve melt processing. In terms of tribological properties, the addition of 30 wt% of PEI into PEEK also produces a material with better scratch hardness (averaging at around 160 MPa based on graphical data) than neat semi-crystalline PEEK (around 125 MPa) and neat PEI (around 65 MPa), likely due to the increased crystallinity of PEEK [177].

Ramani and Alam [178] investigated the thermal and thermo-oxidative degradation kinetics of PEEK/PEI blends over a wide range of compositions. Although the degradation mechanism was different in air and in argon with notable differences especially at high temperature, the results of the thermogravimetric analysis showed a two-stage decomposition process for all the examined blends. The thermal stability of the blend, quantified through the maximum decomposition temperature, T_{max}, of the first degradation step, was proved to depend on the concentration of PEI. Adding PEI progressively reduced T_{max}, with the exception of the 50:50 (wt:wt) blend, whose T_{max} peaked at a value close to neat PEEK (between 568 and 599 °C in argon, and between 567 and 583 °C in air, depending on the heating rate) both in air and in argon [178,179]. The thermal stability of the 50:50 blend was attributed to PEI molecules slowing down the degradation processes within the amorphous phase of the blend. As for the second degradation step, the effect of PEI was negligible in argon, as the second degradation step in argon was very mild for all compositions. However, when the test was repeated in air, it was observed that PEI had the effect of increasing the thermo-oxidative rate of PEEK. This was due to the presence of PEI raising the proportion of the amorphous phase within the polymer blend, which permitted the diffusion of oxygen thus enhancing thermo-oxidation [178]. Limiting the thermo-oxidative rate in PEEK/PEI blends can be achieved through the addition of appropriate additives, like the addition of 1 wt% of organophosphonite antioxidant, Irgafos P-EPQ [180].

Adding titanium dioxide (TiO_2) is an effective way to toughen, stiffen and strengthen PEEK/PEI blends [181]. For example, the specific wear rate of a 70:30 PEEK/PEI blend in dry conditions was measured at ~1.3 × 10^{-5} mm^3/N•m, which was already lower than that of the pure polymers (~2.5 × 10^{-5} and 10.0 × 10^{-5} mm^3/N•m for PEEK and PEI, respectively). The addition of 4 wt% of TiO_2 led to a further ~10-fold decrease. PEI acts as a coupling agent between PEEK and TiO_2, since PEI establishes π–π stacking and polar interactions with PEEK, and hydrogen bonding with TiO_2 [181]. Other examples of composites using PEEK/PEI as a matrix include the reinforcement of PEEK/PEI with 1 wt% of modified halloysite nanotubes (mHNTs) to improve mechanical properties like hardness (from 105 ± 4 to 112 ± 3 Rockwell hardness, M−scale), and flexural, tensile and impact strength (from 160.4 ± 3 to 176.3 ± 2 MPa, from 100.5 ± 2.5 to 114.5 ± 2.2 MPa, and from 53.2 ± 2.2 to 65.5 ± 2.0 kJ m^{-2}, respectively) [182]. Alumina (Al_2O_3)-stabilised PEEK/PEI has been shown to retain dimensional stability above 300 °C [183].

Several contributions in the literature elaborate on the addition of LCP to PEEK/PEI blends. According to Bretas and Baird [184], LCP had limited miscibility in both PEI and PEEK. Nonetheless, its addition to produce a 40%:40%:20% (PEI/PEEK/LCP) blend resulted in an ultimate tensile strength of 110.32 MPa, which is 11% higher than that of neat LCP, 33% higher than that of neat PEEK, and 13% higher than that of neat PEI. LCP also has the effect of lowering the viscosity of PEEK/PEI blends [185]. Blending PEEK/PEI with semi-crystalline meta-linked poly (etherdiphenyl ether ketone) (PEDEKm) led to a rare instance of completely miscible ternary blend (or a three-polymer phase blend) [186].

6.1.3. PEEK/polytetrafluoroethylene (PTFE)

PTFE is popular for low friction applications. Because of its high viscosity and resistance to heating, it cannot be normally processed using conventional melt processing techniques [187,188]. However, PTFE in powder form can be incorporated into melt processable HPPs to produce polymer blends with low friction coefficients. When PTFE is blended into PEEK, the outcome is a blend that is immiscible over a range of PEEK/PTFE compositions. Nonetheless, each composition has excellent tribological properties, and the lowest average coefficient has been registered for samples having 50 wt% of PTFE (0.111, against 0.132 for neat PTFE on lapped stainless steel with a nominal contact pressure of 6.35 MPa) [177]. The optimum PEEK-to-PTFE ratio depends on the targeted property. For example, Hufenbach et al. [189] compared PEEK/PTFE blends containing from 7.5 wt% up to 30 wt% of PTFE and recommended adding 7.5 wt% of PTFE for minimizing the wear rate (with a reduction by 30 times), and 30 wt% for minimizing the friction coefficient (from 0.55 to 0.12 on steel under a pressure of 20 MPa). In addition, PTFE (which has low surface energy) facilitates the extrusion of PEEK even at low concentrations (1–5 wt% of PTFE), because PTFE accumulates on the surface of the melt and lowers the shear forces along the walls of the heated die [190,191].

A more melt processable version of PTFE has also been used in PEEK/PTFE blends. This version of PTFE is obtained by irradiating high molecular weight (conventional) PTFE powder into low molecular weight PTFE (melt processable PFTE, MP-PTFE). By having lower viscosity, MP-PTFE is more suitable than conventional PTFE for melt processing [192]. However, PEEK/MP-PTFE blends are immiscible over every composition [193]. This immiscibility was reasoned to be the cause of the poor mechanical strength of PEEK/MP-PTFE blends since any addition of MP-

PTFE to PEEK led to a reduction in ultimate tensile strength, which dropped from (indicatively) 80–90 MPa for neat PEEK (depending on the processing conditions) to about 10 MPa for the blend with 80 wt% of PTFE (which was even lower than the strength of neat PTFE, i.e., around 25 MPa). To improve the tensile strength, Frick et al. [193] utilized reactive melt extrusion to produce a masterbatch consisting of MP-PTFE treated with electron beam radiation and PEEK in a 50:50 (wt:wt) proportion. The masterbatch was then incorporated into various combinations of PEEK and untreated MP-PTFE. This was shown to reduce the size of the individual polymer domains in the final blends with a 50:50 (wt:wt) or higher proportion of MP-PTFE, but was unable to improve the tensile stress at break in blends containing 80 wt% of PEEK. For the 50:50 blends, the addition of 5 wt% electron beam radiated MP produced an increment of about 40% in stress at break over the base 50:50 blend [193].

In the research conducted by Peng et al. [194,195], the addition of 5 to 7 wt% of Al_2O_3 imparted excellent tribological properties to PEEK/PTFE blends. Chopped glass fibres (1 to 5 wt%) were also shown to increase tensile strength, impact strength, and elastic modulus of a PEEK/(10 wt%) PTFE blend. The addition of 1 wt% of potassium titanate whiskers (PTW) to the same PEEK/(10 wt%) PTFE blend reduced the friction coefficient and wear rate by 7.2% and by 21%, respectively [196]. Other fillers that have been added to PEEK/PTFE blends include alumina nanowires (5 wt%) [197], short carbon fibres and graphite flakes [198,199], and carbon fibre (CF)/graphite [200].

6.1.4. Other PEEK blends

According to Krishnaswamy and Kalika [201], bisphenol-A polyarylate drastically slows down the crystallization rate of PEEK. Similarly, adding 30 wt% of PEKK to PEEK can significantly reduce the crystallization rate of PEEK [114]. PEEK/TPI blends can be compatibilized with an addition of 5 wt% of poly (ether ether ketone)-block-polyimide copolymers (PEEK-b-PI) [202]. The immiscibility of PEEK/TPI blends was harnessed to enable the selective localisation of carbon black particles, which enhanced the electrical properties of the composite with relatively low filler loadings [203].

6.2. PEKK-based blends

6.2.1. PEKK/PEI

PEKK, like PEEK, can produce a miscible blend with PEI, with the advantage (for FFF printing) that PEKK has a slower crystallization rate compared with PEEK [204]. According to the results published by Hsiao and Sauer [205], if PEEK/PEI and PEKK/PEI blends are compared, the crystallization rate is decreased by adding PEI in both systems whenever the poly (aryl ether ketone) is the major phase. However, the temperature corresponding to the maximum crystallization rate increased with the PEI concentration in PEEK/PEI blends, but it decreased in PEKK/PEI blends. This indicated a difference in the crystallization behaviour between PEEK/PEI and PEKK/PEI blends. For both PEEK- and PEKK-based blends, the crystal growth rate decreased with increasing PEI concentration. However, while the nucleation rate in PEEK/PEI blends also decreased on adding PEI, the nucleation rate in PEKK/PEI blends did not depend on the PEI concentration as the growth rate did. This was attributed to the slow crystallization rate of PEKK, and also to the reduction of nucleation density due to the presence of PEI in the amorphous phase of the blend [205].

6.2.2. PEKK/Poly(imide)

Interestingly, PEKK and PEI are miscible in most cases as evidenced by the existence of a single Tg, which varies between the Tg of PEKK (around 159 °C) and that of PEI (around 220 °C) [206,207]. In fact, PEKK was ranked highest for compatibility with TPI when it was compared with other semi-crystalline poly (aryl ether ketone)s (namely, PEEK and polyether ketone ((PEK)) [208]. This was surmised to the similarities between the chain structures of TPI and PEKK, which may encourage dipole–dipole and hydrogen bonding interactions [208].

6.2.3. PEKK/LCP

While PEEK and LCP are shown to be immiscible regardless of the blend composition [209] , PEKK and thermotropic LCP can produce a compatible blend. The addition of thermotropic LCP was proved to ease the melt processability of PEKK. Blending with LCP also increased the tensile strength (from 103.9 ± 2.0 MPa for neat PEKK to 117.8 ± 4.0 MPa for the 7:3 blend), but reduced the elongation at break (from 93.2 ± 1.9% for neat PEKK to 5.2 ± 0.3% for the 7:3 blend) with respect to neat PEKK [210].

6.3. PEI-based blends

6.3.1. PEI/PC

PEI and PC mostly produce immiscible blends with a lower viscosity than pristine PEI [211]. Cicala et al. [212] compared the commercial PEI/PC filament known as ULTEM 9085 with experimental PEI/PC blends and found that, if the material was processed by injection moulding, 20 wt% of PC in the blend was sufficient to sensibly reduce the Tg of the PEI-rich regions from (indicatively) 215 °C to (indicatively) 210 °C. Meanwhile, the tensile modulus and strength of the experimental blends decreased with increasing values of PC content. However, for PC contents up to 40 wt%, the PEI/PC blends showed equal or higher tensile properties compared to ULTEM 9085 counterparts. Similarly, Chun et al. [213] melt-blended PEI and PC and observed that the lowest Tg (around 487 K, nearly 193 °C) was achieved when the concentration of PC was 10 wt%. A separate study used the Flory-Huggins interaction parameter and estimated that the concentration of PEI corresponding to the lowest molar enthalpy and Gibbs free energy change upon mixing the two polymers was 80 wt% [214]. Accordingly, these authors found that there is some partial miscibility when the concentration of PEI in the polymer blend is higher than that of PC [214].

6.3.2. PEI/PAs

Partially miscible blends of PEI and polyamide 6,6 (PA6,6) have been designed in an attempt to lower the viscosity of PEI, making it easier to process in the molten state [215]. However, the sensible difference in viscosity between the two polymers results in poor phase dispersion in the blend [216]. Therefore, to improve the phase dispersion, PA6,6 was replaced with a higher viscosity modified PA (a-PA), having a completely amorphous structure (specifically, poly (trimethyl hexamethylene terephthalamide)). In this way, the viscosity of PEI was reduced by nearly 80% with the addition of a-PA by 20 wt% [216]. To improve on this, poly(ethylene terephthalate) (PET) was incorporated into the blend by first blending 20 wt% of PET into PEI, and then blending again with a-PA to produce a ternary blend [217]. This resulted in a significant refinement of the PEI domains in the blend thanks to the reduced interfacial tension, as demonstrated with contact angle measurements.

6.3.3. PEI/polybutylene terephthalate (PBT)

PEI/PBT blends are partially miscible blends whose mechanical strength is strongly affected by the interfacial region between PEI and PBT. Vásquez-Rendón and Álvarez-Láinez [218] suggested that PEI and PBT should be blended in a 50:50 wt ratio in order to maximise the elongation at break (16.8 ± 4.0%) of the blend, although the ductility is still lower than that of neat PBT (41.0 ± 5.4) than that of neat PEI (26.6 ± 10.4). However, the processability of the blend is known to improve with the presence of PBT [219]. For blends containing 70 and 80 wt% of PEI, the impact resistance was increased by 82% and 118%, respectively, when PTFE was added by 15 wt% as an impact modifier (acting like a rubbery modifier) [220].

6.3.4. PEI/LCP

When PEI (specifically ULTEM 1000 as Stratasys' trade name for PEI

injection moulding grade polymer) is blended with LCP K161, a significant improvement in processability can already be observed after adding as little as 5–10 wt% of LCP [221]. Additionally, if the blend is produced by melt-blending in an extruder, the homogeneity of the phase distribution can be improved (specifically, the size of the LCP phases within the PEI/LCP blend can be reduced) progressively with multiple passes through the extruder [222]. Compatibilizers like polyphosphazene [223] and fillers like silicon carbide-modified multiwalled carbon nanotubes [224], silicon carbide and titanium dioxide-coated multiwalled carbon nanotubes (MWCNTs) [225] or a combination of silicone carbide-modified MWCNTs and polyphosphazene [226] can enable some degree of compatibility between the otherwise immiscible PEI and LCP. Polyesterimide (PEsI) is another compatibilizer which makes it possible to control the size of the LCP islands within the PEI matrix since PEsI can dissolve into both PEI and LCP phases and can reduce the size of the domains of whichever polymer is the minor phase of the blend [227].

6.3.5. Other PEI blends

Other examples of PEI-based HPP blends include the addition of an amorphous copolyester (a-PCTG). In the contribution by Granado et al. [228], blending a-PCTG reduced the viscosity of PEI over the whole compositional range in exam (0–40 wt% of PCTG), with the lowest melt pressure at the exit of the extruder (an index of "processability") being (indicatively) 12 bar for 40 wt% of PCTG. As a term of comparison, the exit pressure for the same blend with 10 wt% of PCTG was (indicatively) 32 bar. Meanwhile, although any addition of a-PCTG to PEI resulted in a decrease in tensile yield strength (nearly linear decrease from (indicatively) 107 MPa for neat PEI to (indicatively) 41 MPa for neat PCTG) and Young's modulus (nearly linear decrease from (indicatively) 3.6 GPa for neat PEI to (indicatively) 1.8 GPa for neat PCTG), there was an improvement in ductility (expressed as the reduction of the transversal area of the tensile sample upon fracture) within all blends. Although the increase in ductility was not linear on composition, it gradually improved from (indicatively) 36% for neat PEI to (indicatively) 48% for the blend with 90 wt% of PCTG. Yet, ductility remained notably lower than what it was observed for neat PCTG (indicatively, 61%).

A miscible blend of PEI and PPSU showed reduced Young's modulus and tensile yield strength over increasing amounts of PPSU. For both properties, the decrease was almost linear from neat PEI (Young's modulus of around 2.6 GPa; strength of around 106 MPa) to neat PPSU (Young's modulus of around 1.95 GPa; strength of around 90 MPa). However, the impact strength was improved compared with unblended PEI. For example, the notch impact strength for a notch radius of 0.25 mm substantially increased from 75 ± 2 J•m for neat PEI to 1033 ± 60 J•m for neat PPSU, with a swift (despite the strong standard deviation) change from 132 ± 20 to 658 ± 300 J•m when the content of PPSU was raised from 30 to 50 wt% [229].

In the study by Blanco et al. [230], the addition of 5 to 10 wt% of polyethylene terephthalate glycol (PETG) was enough to reduce the Tg within PEI/PETG blends with respect to neat PEI by 11 °C, from 208 to 197 °C, which may have some favourable implications for easing processability, although this aspect was not explicitly explored.

6.4. PPS-based blends

6.4.1. PPS/PTFE

Similar to PEEK/PTFE blends (section 6.1.3), the addition of PTFE to PPS has the effect of improving friction and wear properties. Also, PTFE provides a barrier to moisture absorption since PTFE has hydrophobic properties [231]. However, the blend can suffer from poor mechanical properties (tensile strength, for example) since PEEK and PTFE are immiscible. To remediate this drawback, adding short carbon has been demonstrated to improve the tensile strength, hardness, and flexural modulus of PPS/PTFE blends fibres [232,233]. In the contribution by Shi et al. [232], adding 20 wt% of carbon fibres to a 4:1 (wt:wt) PPS/PTFE blend led to the lowest friction coefficient of about μ = 0.103 under the dry-sliding condition. According to the results published by Luo et al. [233], the average friction coefficient and the specific wear rate of a 85:15 (vol:vol) PPS/PTFE blend reinforced by 15 vol% of CF were 0.085 and 5.2×10^{-6} mm^3/Nm, respectively, which were 47% and 88% lower than those of the base PPS/PTFE blend under the same sliding condition.

A synergistic effect was also demonstrated when micro-fibrillated PA6,6 was added to obtain a composite with PPS (56 wt%)/PA (24 wt %)/PTFE (20 wt%). After annealing at 150 °C for 1 h, the friction coefficient and the specific wear rate were as low as 0.139 and 4.372×10^{-6} mm^3/Nm, which were nearly 80% and 1.83×10^3 times lower than those of pure PPS, respectively [234].

6.4.2. PPS/PC

PPS and amorphous PC form partially miscible (compatible) blends. One of the major consequences of blending PPS with PC is the reduced crystallization rate. This is because PC has higher melt viscosity than PPS. Additionally, the presence of PC hinders the motion of PPS chains in regions where the PPS/PC blend is partially miscible, and this hampers the crystallisation of PPS [235]. This reduction in crystallinity in PPS/PC blends with increasing PC proportions was observed, among others, by Lim et al. [236], who also reported on a reduction in the melt viscosity at high temperature. This was the result of the thermal degradation of PC, whereby the average molecular weight of PC decreased from 30,400 to 4900 g/mol. The presence of PC also reduced the Tm of PPS, which dropped from 297.7 to 277.9 °C with an addition of 10 wt% of PC. Likewise, adding PC also reduced the resistance to thermal degradation as the PPS/PC blends had lower onset decomposition temperatures with respect to neat PPS. To illustrate, while the temperature for initial decomposition (in nitrogen) of neat PPS was 460.0 °C, this value dropped to 240.0 °C for the blend containing 60 wt % of PC, which was even lower than that of neat PC (400.0 °C) [237].

The potential disadvantages coming from the thermal degradation of PC may be remediated by melt-blending PPS and PC with epoxy resin (between 2 and 14 phr) to obtain a ternary PPS/PC/epoxy blend. Epoxy acts as a compatibilizer and decreases the interfacial tension between PC and PPS, which results in improved tensile properties compared with blends containing no epoxy. For example, adding 5 phr of epoxy to a 75:25 (wt:wt) PPS/PC blend increased the tensile strength from (indicatively) 26 MPa to (indicatively) 48 MPa. Moreover, epoxy is able to recover the molecular weight of thermally degraded PC, because epoxy reacts with the hydroxyl groups that are present at the ends of the PC chains as a result of hydrolysis upon melt-blending with PPS [238]. The warping and distortion behaviour of PPS/PC blends can also be reduced when PPS/PC blends are combined with appropriate fillers, such as nanosized calcium carbonate (nano-$CaCO_3$) and glass fibers (GF) [239].

6.4.3. PPS/PES

PPS and PES mainly form immiscible blends with some level of compatibility [240], since a small portion of PES may dissolve into the amorphous region of PPS, which results in a decrease in the Tg of the PPS/PES blend [241]. In addition, since neat PES has much higher mechanical properties like tensile, flexural and impact strength compared with neat PPS, blended PPS/PES samples have higher mechanical properties over neat PPS. For instance, the impact strength of PPS has been shown to improve from 2.2 to 3.23 kJ/m^2 when 20 wt% of PES is added to PPS [242].

In order to refine the PES domains dispersed in the PPS matrix, compatibilization of the PPS/PES blend was achieved with the addition of 3 wt% of a hydroxy-functionalized PPS grade. This resulted in a slight improvement of the tensile strength and modulus. Importantly, the compatibilizer was able to improve the storage modulus of a 60:40 (wt:wt) PPS/PES blend over the whole temperature range between 160 and approx. 220 °C, indicating greater thermal stability over the unmodified blend [243]. Another way to improve compatibility is to induce the in-

situ polymerization of a monomer reactant–type polyimide (POI) at the PPS-PES interface. This component is a thermally crosslinkable precursor, which can form a network (via crosslinking or grafting) in the interfacial regions between PPS and PPE, resulting in improved interfacial adhesion [244]. Another method is to use modified PPS that contains a functional phenolphthalein side group attached to a carbon atom on the main chain of PPS. The interaction between this side group and PES molecules can improve the interaction between the two polymers [245].

6.4.4. PPS/PAs

According to Chen et al. [246], the relative amount of PPS and PA into an immiscible blend should be finely tuned to maximise different mechanical properties. For instance, blending 30 wt% of PA6,6 into PPS increases the Rockwell hardness from 86.0 to 92.8 HRM. However, the best values of tensile strength (80.0 MPa), flexural strength (109 MPa), and impact strength (4.9 kJ/m^2) were all achieved by the blend with 70 wt% of PA6.6 [247]. When PPS is blended with a completely amorphous PA (between 10 and 30 wt%), the melting point of the blend is slightly reduced relative to neat PPS (from 301 to 292 °C at 30 wt%). The presence of amorphous PA is known to facilitate the isothermal crystallization of PPS [248]. However, it is unclear how the crystallisation of PPS would be affected in non-isothermal conditions like FFF.

Akhtar and White [249] explored the effect of blending many different varieties of PAs into PPS including PA6, PA11, PA12, PA6,6, and also two forms of aromatic PAs (known by their trade names as Zytel 330 and Grilamid TR 55). In every blend with PPS as the major phase, the tensile strength was reduced or remained the same as neat PPS. However, the elongation at break was enhanced from 5 to 11% in blends containing PA12, although it was not understood why this occurred [249].

The immiscibility of PPS with 10 wt% of PA6,6, which produces a sea-island phase morphology, was exploited to enable specific localisation of carboxyl-modified carbon nanotubes at the interface between the PPS matrix and the PA6,6 domains. The presence of carbon nanotubes hindered the movement of PA6,6 molecules, and this reduced crystallinity and related shrinkage upon cooling [250]. Another study demonstrated that, when clay (between 1 and 10 phr) was added to a PPS/PA6,6 (60:40 wt:wt) blend, the sea–island structure transformed into a co-continuous structure with preferential migration of the clay into PA6,6. Concomitantly, the tensile strength of the blend increased by 10 MPa (+24%) just by adding 1 wt% clay, and by 15 MPa (+35%) when the clay content was raised to 5 wt%, [251].

6.4.5. PPS/PEEK

PPS and PEEK form immiscible semi-crystalline/semi-crystalline polymer blends. According to Mai et al. [252], when PPS is blended with PEEK and then crystallised from the amorphous phase, the double endotherm peak of PPS detected by differential scanning calorimetry (DSC) shifts to lower temperature due to the presence of PEEK. Moreover, the upper melting peak (which is representative of the heat of fusion) decreases significantly and a third peak may also appear depending on the thermal history. If PPS/PEEK blends are crystallized under non-isothermal conditions, PEEK increases the maximum crystallization temperature and the crystallisation rate of PPS, which suggests that PEEK acts as a nucleation agent for PPS [253].

PPS/PEEK blends can be turned into miscible blends with the addition of PEI, where the single Tg value of PEEK/PPS/PEI ternary blends increases from 146 °C to 179 °C when the amount of PEI and PPS is raised from 5 to 35 wt% [254]. Trisilanolphenyl polyhedral oligomeric silsesquioxane (Tsp-POSS) is able to reduce the melt flow of both PEEK and PPS without affecting their impact and tensile strength. However, the role of tsp-POSS has not been tested on PEEK/PPS blends [255]. A PPS/PEEK blend produced with recycled PEEK was functionalised with carbon nanotubes, which improved the compatibility between PEEK and PPS, and increased the flexural modulus by 24% (at 20 wt% of CNTs) over neat PPS (modulus of neat PPS: 3200 ± 20.9 MPa) [256]. The improvement in interfacial compatibility between the polymer phases was attributed to the localisation of carbon nanotubes, which preferentially migrated into the PPS matrix and concentrated in the interface between PPS matrix and PEEK islands, acting as an inorganic compatibilizer [256].

6.4.6. Other PPS blends

As with PTFE, friction coefficient (from 0.80 to 0.20) and wear properties (wear rate, from 7.14 × 10^{-5} to 8.16 × 10^{-7} mm^2/(Nm)) of PPS can be ameliorated by adding 10 wt% of LDPE [257]. Although PPS/poly(2-vinylpyridine) (PVP) are generally classified as immiscible, it has been suggested that the two polymers become partially miscible upon increasing the PVP fraction in the blend. Crystallization can be delayed in PPS with the addition of 5 wt% of PVP, which reduces the nucleation rate of PPS and slows down the growth rate of the spherulites [258]. An addition of 5 wt% of polyvinylidene fluoride (PVDF) into PPS produces an immiscible structure that increases the tensile strength of neat PPS from 33.3 to 53.7 MPa, and the tensile modulus from 1140.2 to 1630.6 MPa [259].

7. Examples of HPP blends in FFF

Although the adoption of polymer blending in FFF is still in its infancy, several examples can already be found in the literature, and some are even commercially available. The following sections provide a summary of the HPP blends that are currently being used in the FFF community.

7.1. PEEK/Amorphous PAEK

Blending 7 wt% of fully amorphous poly-aryl-ether-ketone (aPAEK) within a PEEK filament improved the interlayer strength of the printed samples by 130% [260]. In fact, aPAEK was able to quickly diffuse to the interlayer region, thus enabling improved polymer welding processes that rely on easier diffusion and disentanglement in the amorphous phase.

7.2. PEEK/PEI

Blends of PEI in a PEEK matrix (100/0, 90/10, 80/20, 70/30, 60/40, 50/50 and 40/60 wt ratios) were reinforced with 30 wt% of chopped carbon fibres in the contribution by Diouf-Lewis et al. [261]. Tensile tests conducted on composite filaments for FFF showed that the 80:20 blend achieved the highest value of the Young's Modulus (13 GPa). Notably, besides the nominal composition of the blend and the addition of chopped carbon fibres, the tensile properties of the filaments were deeply affected by the presence of pores. As a matter of fact, the reinforced 80:20 blend also exhibited the lowest degree of porosity (2.90%) among all systems in exam.

7.3. PEI/oligophenylene sulfone (OPSU)

Slonov et al. [262] investigated the effect of blending oligophenylene sulfone (OPSU) with PEI and compared the obtained PEI/OPSU blends to PEI/PC blends. Although it was observed that OPSU produces a miscible blend, while the combination of PEI/PC is immiscible, both OPSU and PC acted as plasticisers and reduced the viscosity of PEI. The tensile and flexural properties of the blends were generally lower than those of neat PEI. However, the blend with 20 wt% of OPSU was an exception, with a tensile strength of 103.8 ± 3.2 MPa, against 88.0 ± 5 MPa of neat PEI. Also, the unnotched impact strength surpassed that of neat PEI (75.5 ± 7.6 kJ/m^2) when the content of PC was 15 wt% or higher (79.5 ± 8.0 kJ/m^2 at 15 wt%; 84.7 ± 8.5 kJ/m^2 at 20 wt%). This was attributed to the high molecular weight and plasticity of PC, which promoted the elasticisation of PEI. OPSU, on the contrary, having a low

MW, caused the samples to become more brittle [262].

7.4. PEI/PC

A popular PEI/PC blend used in FFF is ULTEM 9085, under the trade name introduced by Stratasys [263]. Cicala et al. [212] compared ULTEM 9085 and experimental PEI/PC blends and found that, when 10 wt% of PC was added to PEI, melt processing became much easier over neat PEI. In terms of mechanical performance, the tensile strength and modulus of the experimental blends outperformed ULTEM 9085 whenever the blends contained between 10 and 40 wt% of PC. However, since ULTEM 9085 is a proprietary blend, whose detailed composition is not publicly available, it is not clear why this occurred [212].

When printing with ULTEM 9085, the thermal environment of the printer chamber is shown to significantly affect the mechanical integrity of the printed part [264]. With careful selection of the g-code parameters, the printed parts can reach a tensile strength relatively close (about 85%) to that of injection moulded parts, which was assumed to be 82.75 MPa [265]. In addition, post processing reduces mechanical anisotropy (by up to 80%) and improves the flexural modulus (by 21%) and strength (by 75%) of ULTEM 9085 printed parts [266].

Hardness can also be increased in ULTEM 9085 printed parts through appropriate setting of the infill direction in alternating patterns [267]. Meanwhile, the printing direction affects the wear resistance. For example, the average weight loss was remarkably higher for samples printed in the "Z" orientation (i.e., layers perpendicular to the direction of wear) than for those printed in the "X" orientation (i.e., layers parallel to the direction of wear).

It is generally acknowledged that moisture absorption in the ULTEM 9085 filament above 0.1 wt% is detrimental to the printing process and the quality of the printed parts [39]. However, slightly different results have been observed for different printing directions. For "XY" samples (printed flat on the build plate), if moisture uptake in the filament does not exceed 0.1%, the melt viscosity upon printing decreases, and this results in a highly consolidated cross section. However, increasing the humidity of the filament above 0.1% leads to diffused porosity and microstructural defects (e.g., inter-strand bond degradation). As a consequence, the stiffness and strength of the "XY" samples increased with moisture uptake up to 0.1% (ultimate tensile strength: from 50.1 $\pm$ 3.0 to 56.8 $\pm$ 1.2 MPa; elastic modulus: from 1.93 $\pm$ 0.02 to 2.04 $\pm$ 0.04 GPa), but then dropped for higher absorbed humidity. Conversely, the tensile stiffness and strength of the "ZX" samples (printed upright) steadily decreased (with the reference values for the control at 0% humidity being: ultimate tensile strength of 35.9 $\pm$ 5.7 MPa; elastic modulus of 2.09 $\pm$ 0.03 GPa), regardless of the amount of absorbed water, which can be attributed to the presence of numerous inter-layer interfaces and to the different temperature profile upon printing [39].

Vakharia et al. [268] printed various multi-material samples made of neat ULTEM 9085 and a composite consisting of ULTEM 9085 blended with short carbon fibres. The cross-sectional analysis of the printed parts revealed that the fibre-reinforced layers had a large amount of apparent porosity: approximately 31%, as compared to the layers with neat ULTEM 9085 (apparent porosity of 2% area). This extensive porosity produced poor adhesion, regardless of the layering sequence. Also, the presence of (brittle) carbon fibres affected the toughness of the composite layers. As a result, multi-material parts with alternating layers of neat ULTEM 9085 and fibre reinforced ULTEM 9085 were able to achieve more strain before failure than those with consecutive ULTEM 9085 layers (0.033 for the ABABAB layering sequence vs. 0.025 mm/mm for the AAABBB layering sequence), most likely due to the toughness of the intercalated ULTEM 9085 layers enabling continued elongation.

One consideration is that, at present, the only dissolvable support available for printing with ULTEM 9085 is a material provided by Stratasys which contains PSU [269]. This polymer is chemically similar to PEI and thus removal of support material using chemical solvents like dimethylformamide has the risk of degrading the ULTEM 9085 part itself. One study suggested that submerging the printed parts for 8 h in pure 1-bromopropane or toluene may be a safe strategy for removing the support material whilst retaining the mechanical properties of the printed part [270].

8. Discussion

PEEK, PEKK, PPS, PEI, TPI, and PPSU are increasingly popular for the FFF of load-bearing components that combine the mechanical strength of HPPs with the freedom in geometry that is typical of AM. While PEEK is most likely the prevalent HPP being currently explored in the literature, it is not possible to prioritise the adoption of HPPs, since each of them comes with specific properties that depend on their chemical make-up, on the establishment of inter-molecular interactions, and on the ability to crystallise. For example, although both PEEK and PEKK are poly(aryl ether ketone)s, the crystallisation rate of PEKK is much lower than that of PEEK. Also, PEKK can crystallise in additional polymorphs [111-114]. Again, while PEEK is highly crystalline, PEI is fully amorphous [271]. Additionally, for a given HPP, the processability and the final properties are deeply affected by the specific chemical structure, by the molecular weight (average value and distribution), and by the thermal history. This justifies the noticeable fluctuations encountered in the literature where, for example, the Young's modulus of PEEK parts produced by FFF can largely vary between (around) 0.3 GPa and (around) 4.1 GPa, and the tensile strength between (around) 10 MPa and (around) 100 MPa, as documented in the review by Zanjanijam et al. [8].

Despite these variations, all HPPs feature outstanding mechanical strength, which can be retained under extreme working conditions. For this reason, HPPs represent the next generation of high-end polymers for FFF. Nonetheless, HPPs are currently underutilised in FFF. This is mainly because HPPs are much more difficult to print than commercial polymers (such as PLA and ABS), and engineering ones (such as nylon). The bulky molecular structure, the presence of numerous aromatic rings, and the formation of extensive inter-molecular bonds that are responsible for the extraordinary mechanical performance of HPPs are also responsible for excessive melt viscosity, sensitivity to moisture uptake, fast crystallization (for semi-crystalline HPPs), and related part distortion and shrinkage.

Also, the mechanical strength of HPP parts produced by FFF may be undermined by poor structural consolidation due to weak inter-strand and inter-layer adhesion. Although FFF does hold some similarity to "conventional" techniques like injection and compression moulding, in that they are all based on melt processing, the strong dependence of structural consolidation on interface welding (namely, raster-raster and layer-layer bonding through polymer sintering and healing) is peculiar to FFF. The achievement of strong interfaces becomes critical for those HPPs that, like PEEK, feature a very high crystallisation rate, because the quick crystallisation prevents effective bonding between adjacent rasters and subsequent layers [46].

In principle, tackling these issues by chemical redesign of HPPs would be feasible, but likely uneconomical, because this would require the formulation, synthesis and scale up of new polymers with specific chemical structures. Meanwhile, tuning the printing parameters is certainly useful to promote structural consolidation, but still insufficient to unleash the full potential of HPPs in FFF. The analysis of the literature shows that polymer blending may be a smarter and more effective avenue of remediating the poor printability of HPPs while also embedding new functionality [272].

Due to its versatility, polymer blending is routinely applied to overcome the limited processability of HPPs in traditional melt-based techniques like injection and compression moulding. With a focus on the HPPs most commonly used in FFF, over 20 different blends have been identified which, in principle, may provide potential improvements to the melt processability of these materials (by reducing viscosity or friction during printing) or imbue/enhance mechanical and

functional properties like tensile strength, hardness, or wear resistance. For example, adding PSU to PEEK reduces the melt viscosity and improves the processability of PEEK while retaining its mechanical strength [162]. Similarly, the viscosity of PEI can be reduced by nearly 80% with the addition of amorphous polyamide [216], while the tensile strength and stiffness of PPS can be increased by nearly 50% by adding just 5 wt% of PVDF [259].

Surprisingly, in spite of the demonstrated success of polymer blending in conventional melt processing methods, only a handful of PEEK- and PEI-based blends have been explored within FFF. This gap mainly originates from historical circumstances, with FFF being much younger than compression and injection moulding. Moreover, the adoption of HPPs in FFF is, by itself, very recent. To illustrate, the first occurrence of FFF of PEEK in Scopus dates back to 2014 (search conducted by entering ("fused filament fabrication" OR "fused deposition modeling") AND (PEEK) in Article title, Abstract, Keywords).

Nowadays, research is rapidly progressing in the field, and the success of polymer blending for the FFF of HPPs is proved by the fact that one printable blend (ULTEM 9085, a proprietary PEI/PC-based filament commercialized by Stratasys [265]) is readily available in the marketplace. In future, the wider adoption of polymer blending is expected to further the utilization of HPPs in FFF, thus bolstering the applicability of this technology both in scientific discovery and in industrial practice. Moreover, the same concept of polymer blending can be extended to improving the printability and mechanical performance of commercial- and engineering-grade polymers that may be otherwise difficult to print with, for example due to their fast crystallisation kinetics [273]. However, researchers in the fields should be aware of possible limitations and challenges associated with polymer blending for FFF, which can be summarised as follows:

- Many advantages afforded by polymer blending have been demonstrated in conventional melt processing techniques, but experimental evidence is still needed to substantiate these benefits in FFF.
- In particular, there is a lack of knowledge concerning TPI and PPSU. Although these HPPs are gaining interest in the FFF community, very little is known about melt blending them, since they are seldom accounted for in the literature about polymer blending in conventional melt processing techniques.
- Oftentimes, for any given combination of polymers, the "best" HPP blend formulation is different depending on the targeted property. This means that the blend composition must be optimised separately for each property, and trade-offs may be required if multiple properties are sought after simultaneously.
- Additional studies should be directed to characterising the interfacial regions and phase dispersion in partially or completely immiscible blends, and to understanding the effect of chemical modification and post-processing treatment.

9. Conclusions

High performance polymers (HPPs) feature outstanding mechanical strength, thermal stability, and chemical resistance. Their adoption in fused filament fabrication (FFF), which is currently the most popular plastic-based additive manufacturing technique, enables the production of advanced components with bespoke geometry for load-bearing applications in aerospace, aviation, and biomedicine. However, the same compositional and structural features that afford their unparalleled functional properties (i.e., bulky and "stiff" polymer chains, high molecular weight, and strong inter-molecular interactions), also make HPPs very difficult to print. Besides the very high processing temperature required, successful printing of HPPs by FFF may be undermined by their extremely high melt viscosity, strong propensity to shrinkage and warpage, and sensitivity to moisture uptake. Furthermore, most HPPs are semi-crystalline polymers with high crystallisation rates, which may impair inter-raster and inter-layer welding. Polymer blending, which consists in mixing two or more polymer together in order to take advantage of the respective properties, is emerging as a practical and convention solution to the printing issues of HPPs. Historically used in "conventional" techniques like injection and compression moulding, the benefit of polymer blending is two-fold, as it facilitates melt processing while also improving the mechanical properties over the base polymers. Although the examples are still rare, the efficacy of polymer blending in FFF is demonstrated by the availability of a commercial filament that combines poly-ether-imide and polycarbonate. While polymer blending holds the promise to advance the FFF of HPPs, additional research is needed to translate the available knowledge from conventional melt processing to 3D printing, and to better manipulate the interface region and phase dispersion in immiscible and compatible blends. In future, a major challenge may be represented by the optimisation of HPP blends, since different functional properties may respond in a different way to compositional changes.

Declaration of Competing Interest

The authors declare that they have no known competing financial interests or personal relationships that could have appeared to influence the work reported in this paper.

Data availability

No data was used for the research described in the article.

Acknowledgments

The Commonwealth Scientific and Industrial Research Organisation (CSIRO) is gratefully acknowledged for providing the necessary materials and capability for this review. AS, DPS, and JJ are supported by CSIRO's Research Office through the 'Science Leader in Active Materials' grant. AEZK is supported by CSIRO's Research Office through the R+CERC Fellowships Program.

References

[1] G. Bhat, V. Kandagor, Synthetic polymer fibers and their processing requirements, Advances in Filament Yarn Spinning of Textiles and Polymers. (2014) 3–30. https://doi.org/10.1533/9780857099174.1.3.
[2] Roboze, MotoGP 2022: Ducati Corse boosts performance with Roboze 3D printing | Roboze, 2022. https://www.roboze.com/en/resources/motogp-2022-ducati-corse-boosts-performance-with-roboze-3d-printing.html (accessed March 27, 2023).
[3] ISO / ASTM52900, Standard Terminology for Additive Manufacturing – General Principles – Terminology, ASTM International. (2021). www.astm.org.
[4] T. Prater, N. Werkheiser, F. Ledbetter, D. Timucin, K. Wheeler, M. Snyder, 3D Printing in Zero G Technology Demonstration Mission: complete experimental results and summary of related material modeling efforts, Int. J. Adv. Manuf. Technol. 101 (2019) 391–417, https://doi.org/10.1007/s00170-018-2827-7.
[5] T. Prater, Q. Bean, N. Werkheiser, R. Grguel, R. Beshears, T. Rolin, T. Huff, R. Ryan, F. Ledbetter, E. Ordonez, Analysis of specimens from phase I of the 3D printing in Zero G technology demonstration mission, Rapid Prototyp. J. 23 (2017) 1212–1225, https://doi.org/10.1108/RPJ-09-2016-0142.
[6] Orion, The First 3D Printed Parts On The Moon, 2022. https://orion-am.com/blog/orion-am-news-1/orion-am-touches-the-moon-17# (accessed March 27, 2023).
[7] A. El Magri, S. Vanaei, S. Vaudreuil, An overview on the influence of process parameters through the characteristic of 3D-printed PEEK and PEI parts, High Perform. Polym. 33 (2021) 862–880, https://doi.org/10.1177/09540083211009961.
[8] A.R. Zanjanijam, I. Major, J.G. Lyons, U. Lafont, D.M. Devine, Fused filament fabrication of peek: A review of process-structure-property relationships, Polymers (Basel) 12 (2020), https://doi.org/10.3390/POLYM12081665.
[9] S. Jiang, G. Liao, D. Xu, F. Liu, W. Li, Y. Cheng, Z. Li, G. Xu, Mechanical properties analysis of polyetherimide parts fabricated by fused deposition modeling, High Perform. Polym. 31 (2019) 97–106, https://doi.org/10.1177/0954008317752822.
[10] K. Rashed, A. Kafi, R. Simons, S. Bateman, Effects of fused filament fabrication process parameters on tensile properties of polyether ketone ketone (PEKK), Int. J. Adv. Manuf. Technol. 122 (2022) 3607–3621, https://doi.org/10.1007/S00170-022-10134-1/TABLES/11.

[11] K. Rodzeń, E. Harkin-Jones, M. Wegrzyn, P.K. Sharma, A. Zhigunov, Improvement of the layer-layer adhesion in FFF 3D printed PEEK/carbon fibre composites, Compos. Part A Appl. Sci. Manuf. 149 (2021), 106532, https://doi.org/10.1016/J.COMPOSITESA.2021.106532.

[12] M.F. Arif, H. Alhashmi, K.M. Varadarajan, J.H. Koo, A.J. Hart, S. Kumar, Multifunctional performance of carbon nanotubes and graphene nanoplatelets reinforced PEEK composites enabled via FFF additive manufacturing, Compos. B Eng. 184 (2020), 107625, https://doi.org/10.1016/J.COMPOSITESB.2019.107625.

[13] K. Rodzeń, M.J. McIvor, P.K. Sharma, J.G. Acheson, A. McIlhagger, M. Mokhtari, A. McFerran, J. Ward, B.J. Meenan, A.R. Boyd, The surface characterisation of fused filament fabricated (Fff) 3d printed peek/hydroxyapatite composites, Polymers (Basel) 13 (2021), https://doi.org/10.3390/POLYM13183117/S1.

[14] P.M. Hergenrother, The use, design, synthesis, and properties of high performance/high temperature polymers: An overview, High Perform. Polym. 15 (2003) 3–45, https://doi.org/10.1177/0954008303015001O1.

[15] C. Duty, C. Ajinjeru, V. Kishore, B. Compton, N. Hmeidat, X. Chen, P. Liu, A. A. Hassen, J. Lindahl, V. Kunc, What makes a material printable? A viscoelastic model for extrusion-based 3D printing of polymers, J. Manuf. Process. 35 (2018) 526–537, https://doi.org/10.1016/j.jmapro.2018.08.008.

[16] E. Boytsov, S. Blaginin, A. Sinkov, Why we Need a Heated Chamber for 3D Printing with 'High Performance' Polymers?, in: Materials Research Proceedings, Materials Research Forum LLC, 2022: pp. 237–246. https://doi.org/10.21741/9781644901755-42.

[17] S. Kumar, R.K. Mishra, T. Nandi, Experimental and theoretical investigations of the high performance blends of PEEK/PEI, J. Polym. Eng. 38 (2018) 351–361, https://doi.org/10.1515/polyeng-2017-0002.

[18] A. Mehta, A.I. Isayev, Rheology, morphology, and mechanical characteristics of poly(etherether ketone)-liquid crystal polymer blends, Polym. Eng. Sci. 31 (1991) 971–980, https://doi.org/10.1002/PEN.760311307.

[19] B.B. Shahriar, C. France, N. Valerie, C. Arthur, G. Christian, Toward improvement of the properties of parts manufactured by FFF (fused filament fabrication) through understanding the influence of temperature and rheological behaviour on the coalescence phenomenon, in: AIP Conf Proc, AIP Publishing LLC AIP Publishing, 2017, p. 040008. https://doi.org/10.1063/1.5008034.

[20] P. Ferretti, C. Leon-Cardenas, G.M. Santi, M. Sali, E. Ciotti, L. Frizziero, G. Donnici, A. Liverani, Relationship between fdm 3d printing parameters study: Parameter optimization for lower defects, Polymers (Basel) 13 (2021), https://doi.org/10.3390/polym13132190.

[21] T.J. Coogan, D.O. Kazmer, Modeling of interlayer contact and contact pressure during fused filament fabrication, J. Rheol. (N Y N Y) 63 (2019) 655–672, https://doi.org/10.1122/1.5093033.

[22] A. Sola, A. Trinchi, Basic principles of fused deposition modeling, Fused Deposition Modeling of Composite Materials (2023) 7–39, https://doi.org/10.1016/B978-0-323-98823-0.00001-9.

[23] C.Y. Liaw, J.W. Tolbert, L.W. Chow, M. Guvendiren, Interlayer bonding strength of 3D printed PEEK specimens, Soft Matter 17 (2021) 4775–4789, https://doi.org/10.1039/D1SM00417D.

[24] X. Gao, S. Qi, X. Kuang, Y. Su, J. Li, D. Wang, Fused filament fabrication of polymer materials: A review of interlayer bond, Addit. Manuf. 37 (2021), 101658, https://doi.org/10.1016/j.addma.2020.101658.

[25] A. Sola, W.J. Chong, D. Pejak Simunec, Y. Li, A. Trinchi, I. (Louis) Kyratzis, C. Wen, Open challenges in tensile testing of additively manufactured polymers: A literature survey and a case study in fused filament fabrication, Polym. Test. 117 (2023), 107859, https://doi.org/10.1016/j.polymertesting.2022.107859.

[26] A.P. Golhin, A. Strandlie, P.J. Green, The Influence of Wedge Angle, Feedstock Color, and Infill Density on the Color Difference of FDM Objects, J. Imaging Sci. Technol. 65 (2021) 1–15, https://doi.org/10.2352/J.IMAGINGSCI.TECHNOL.2021.65.5.050408.

[27] A.E. Costa, A. Ferreira da Silva, O. Sousa Carneiro, A study on extruded filament bonding in fused filament fabrication, Rapid Prototyp. J. 25 (2019) 555–565, https://doi.org/10.1108/RPJ-03-2018-0062/FULL/XML.

[28] D. Vaes, M. Coppens, B. Goderis, W. Zoetelief, P. Van Puyvelde, The extent of interlayer bond strength during fused filament fabrication of nylon copolymers: An interplay between thermal history and crystalline morphology, Polymers (Basel) 13 (2021) 2677, https://doi.org/10.3390/polym13162677.

[29] Q. Sun, G.M. Rizvi, C.T. Bellehumeur, P. Gu, Effect of processing conditions on the bonding quality of FDM polymer filaments, Rapid Prototyp J. 14 (2008) 72–80, https://doi.org/10.1108/13552540810862028/FULL/PDF.

[30] D. Pejak Simunec, A. Sola, Emerging Research in Conductive Materials for Fused Filament Fabrication: A Critical Review, Adv. Eng. Mater. 24 (2022) 2101476, https://doi.org/10.1002/ADEM.202101476.

[31] N.P. Levenhagen, M.D. Dadmun, Bimodal molecular weight samples improve the isotropy of 3D printed polymeric samples, Polymer (Guildf) 122 (2017) 232–241, https://doi.org/10.1016/j.polymer.2017.06.057.

[32] N.P. Levenhagen, M.D. Dadmun, Interlayer diffusion of surface segregating additives to improve the isotropy of fused deposition modeling products, Polymer (Guildf) 152 (2018) 35–41, https://doi.org/10.1016/j.polymer.2018.01.031.

[33] T.J. Gordelier, P.R. Thies, L. Turner, L. Johanning, Optimising the FDM additive manufacturing process to achieve maximum tensile strength: a state-of-the-art review, Rapid Prototyp J. 25 (2019) 953–971, https://doi.org/10.1108/RPJ-07-2018-0183/FULL/XML.

[34] C.C. Shih, M. Burnette, D. Staack, J. Wang, B.L. Tai, Effects of cold plasma treatment on interlayer bonding strength in FFF process, Addit. Manuf. 25 (2019) 104–111, https://doi.org/10.1016/J.ADDMA.2018.11.005.

[35] M.F. Arif, S. Kumar, K.M. Varadarajan, W.J. Cantwell, Performance of biocompatible PEEK processed by fused deposition additive manufacturing, Mater. Des. 146 (2018) 249–259, https://doi.org/10.1016/J.MATDES.2018.03.015.

[36] R.H. Colby, L.J. Fetters, W.W. Graessley, Melt Viscosity-Molecular Weight Relationship for Linear Polymers, Macromolecules 20 (1987) 2226–2237, https://doi.org/10.1021/MA00175A030/ASSET/MA00175A030.FP.PNG_V03.

[37] J. Go, S.N. Schiffres, A.G. Stevens, A.J. Hart, Rate limits of additive manufacturing by fused filament fabrication and guidelines for high-throughput system design, Addit. Manuf. 16 (2017) 1–11, https://doi.org/10.1016/J.ADDMA.2017.03.007.

[38] I. Baek, O. Kwon, C.M. Lim, K.Y. Park, C.J. Bae, 3D PEEK Objects Fabricated by Fused Filament Fabrication (FFF), Materials 15 (2022) 898, https://doi.org/10.3390/ma15030898.

[39] R.J. Zaldivar, T.D. Mclouth, G.L. Ferrelli, D.N. Patel, A.R. Hopkins, D. Witkin, Effect of initial filament moisture content on the microstructure and mechanical performance of ULTEM® 9085 3D printed parts, Addit. Manuf. 24 (2018) 457–466, https://doi.org/10.1016/J.ADDMA.2018.10.022.

[40] A.D. Banjo, V. Agrawal, M.L. Auad, A.D.N. Celestine, Moisture-induced changes in the mechanical behavior of 3D printed polymers, Compos. Part C: Open Access. 7 (2022), 100243, https://doi.org/10.1016/J.JCOMC.2022.100243.

[41] D. Vaes, P. Van Puyvelde, Semi-crystalline feedstock for filament-based 3D printing of polymers, Prog. Polym. Sci. 118 (2021), 101411, https://doi.org/10.1016/j.progpolymsci.2021.101411.

[42] A. Shrivastava, Plastics Processing, in: Introduction to Plastics Engineering, William Andrew Publishing, 2018, pp. 143–177. https://doi.org/10.1016/b978-0-323-39500-7.00005-8.

[43] A. Rozanski, A. Galeski, Plastic yielding of semicrystalline polymers affected by amorphous phase, Int. J. Plast. 41 (2013) 14–29, https://doi.org/10.1016/J.IJPLAS.2012.07.008.

[44] T. Choupin, B. Fayolle, G. Régnier, C. Paris, J. Cinquin, B. Brulé, A more reliable DSC-based methodology to study crystallization kinetics: Application to poly (ether ketone ketone) (PEKK) copolymers, Polymer (Guildf) 155 (2018) 109–115, https://doi.org/10.1016/J.POLYMER.2018.08.060.

[45] Y. Shang, Q. Xu, B. Jiang, Y. Yang, X. Liu, Z. Jiang, C. Yu, X. Li, H. Zhang, Slowing crystallization to enhance interlayer strength of 3D printed poly (ether ether ketone) parts by molecular design, Addit. Manuf. 59 (2022), 103104, https://doi.org/10.1016/J.ADDMA.2022.103104.

[46] D.W. Collinson, N. von Windheim, K. Gall, L.C. Brinson, Direct evidence of interfacial crystallization preventing weld formation during fused filament fabrication of poly(ether ether ketone), Addit. Manuf. 51 (2022), 102604, https://doi.org/10.1016/J.ADDMA.2022.102604.

[47] A. Das, E.L. Gilmer, S. Biria, M.J. Bortner, Importance of Polymer Rheology on Material Extrusion Additive Manufacturing: Correlating Process Physics to Print Properties, ACS Appl. Polym. Mater. 3 (2021) 1218–1249, https://doi.org/10.1021/ACSAPM.0C01228/ASSET/IMAGES/LARGE/AP0C01228_0011.JPEG.

[48] E.L. Gilmer, D. Miller, C.A. Chatham, C. Zawaski, J.J. Fallon, A. Pekkanen, T. E. Long, C.B. Williams, M.J. Bortner, Model analysis of feedstock behavior in fused filament fabrication: Enabling rapid materials screening, Polymer (Guildf). 152 (2018) 51–61, https://doi.org/10.1016/j.polymer.2017.11.068.

[49] J. Dealy, K. Wissbrun, Melt rheology and its role in plastics processing: theory and applications, Springer Science & Business Media, 2012. https://books.google.com/books?hl=en&lr=&id=_3HrCAAAQBAJ&oi=fnd&pg=PA1&ots=vsq9S_cX3f&sig=Lll7E9TlnS0sESSQzhG0kBCFGDM (accessed February 28, 2023).

[50] N. Venkataraman, S. Rangarajan, M.J. Matthewson, B. Harper, A. Safari, S. C. Danforth, G. Wu, N. Langrana, S. Guceri, A. Yardimci, Feedstock material property - Process relationships in fused deposition of ceramics (FDC), Rapid Prototyp J. 6 (2000) 244–252, https://doi.org/10.1108/13552540010373344/FULL/XML.

[51] N. Venkataraman, S. Rangarajan, M.J. Matthewson, A. Safari, S.C. Danforth, A. Yardimci, Mechanical and rheological properties of feedstock material for fused deposition of ceramics and metals (FDC and FDMet) and their relationship to process performance, Solid Freeform Fabrication Proceedings 1999 (August 1999) 351–359. https://doi.org/10.26153/TSW/827.

[52] L. Fang, Y. Yan, O. Agarwal, S.H. Kang, S. Yao, J.E. Seppala, Effects of environmental temperature and humidity on the geometry and strength of polycarbonate specimens prepared by fused filament fabrication, Materials 13 (2020) 1–16, https://doi.org/10.3390/ma13194414.

[53] P. Geng, J. Zhao, W. Wu, W. Ye, Y. Wang, S. Wang, S. Zhang, Effects of extrusion speed and printing speed on the 3D printing stability of extruded PEEK filament, J. Manuf. Process. 37 (2019) 266–273, https://doi.org/10.1016/J.JMAPRO.2018.11.023.

[54] Y. Chikahisa, A theory on the relationship between viscosity and molecular weight in bulk polymers, J. Phys. Soc. Japan 19 (1964) 92–100, https://doi.org/10.1143/JPSJ.19.92.

[55] J.D. Roberts, M.C. Caserio, Chapter 29. Polymers, Basic Principles of Organic Chemistry. (1977) 1419–1459. http://resolver.caltech.edu/CaltechBOOK:1977.001%5Cnhttp://authors.library.caltech.edu/25034/30/BPOCchapter29.pdf (accessed March 28, 2023).

[56] C. Schaller, 4.2: Viscosity of Polymers - Chemistry LibreTexts, Structure & Reactivity in Organic, Biological and Inorganic Chemistry. (2021) 1–4. https://chem.libretexts.org/Bookshelves/Organic_Chemistry/Polymer_Chemistry_(Schaller)/04%3A_Polymer_Properties/4.02%3A_Viscosity (accessed March 28, 2023).

[57] C. Ajinjeru, V. Kishore, P. Liu, A.A. Hassen, J. Lindahl, V. Kunc, C. Duty, Rheological evaluation of high temperature polymers to identify successful extrusion parameters, Solid Freeform Fabrication 2017: Proceedings of the 28th

Annual International Solid Freeform Fabrication Symposium - An Additive Manufacturing Conference, SFF 2017. (2020) 485–494.
[58] J.W. Tseng, C.Y. Liu, Y.K. Yen, J. Belkner, T. Bremicker, B.H. Liu, T.J. Sun, A. B. Wang, Screw extrusion-based additive manufacturing of PEEK, Mater. Des. 140 (2018) 209–221, https://doi.org/10.1016/j.matdes.2017.11.032.
[59] B.N. Panda, K. Shankhwar, A. Garg, Z. Jian, Performance evaluation of warping characteristic of fused deposition modelling process, Int. J. Adv. Manuf. Technol. 88 (2017) 1799–1811, https://doi.org/10.1007/s00170-016-8914-8.
[60] U. Yaman, Shrinkage compensation of holes via shrinkage of interior structure in FDM process, Int. J. Adv. Manuf. Technol. 94 (2018) 2187–2197, https://doi.org/10.1007/s00170-017-1018-2.
[61] Y. Wang, W.D. Müller, A. Rumjahn, A. Schwitalla, Parameters influencing the outcome of additive manufacturing of tiny medical devices based on PEEK, Materials 13 (2020), https://doi.org/10.3390/ma13020466.
[62] X. Wei, D. Li, W. Jiang, Z. Gu, X. Wang, Z. Zhang, Z. Sun, 3D Printable Graphene Composite, Sci. Rep. 5 (2015) 1–7, https://doi.org/10.1038/srep11181.
[63] S.V. Kondrashov, A.A. Melnikov, M.A. Gusev, D.A. Gurov, P.A. Shchur, Investigation of the effect of nozzle temperature on the properties of polyethylene samples obtains by FDM printing, High Temp. Mater. Processes (New York) 27 (2023) 21–29, https://doi.org/10.1615/HighTempMatProc.2022044718.
[64] C. Yang, X. Tian, D. Li, Y. Cao, F. Zhao, C. Shi, Influence of thermal processing conditions in 3D printing on the crystallinity and mechanical properties of PEEK material, J. Mater. Process Technol. 248 (2017) 1–7, https://doi.org/10.1016/j.jmatprotec.2017.04.027.
[65] W.Z. Wu, P. Geng, J. Zhao, Y. Zhang, D.W. Rosen, H.B. Zhang, Manufacture and thermal deformation analysis of semicrystalline polymer polyether ether ketone by 3D printing, Mater. Res. Innov. 18 (2014), https://doi.org/10.1179/1432891714Z.000000000898. S5–12-S5-16.
[66] A.A. Rosli, R.K. Shuib, K.M.K. Ishak, Z.A.A. Hamid, M.K. Abdullah, A. Rusli, Influence of bed temperature on warpage, shrinkage and density of various acrylonitrile butadiene styrene (ABS) parts from fused deposition modelling (FDM), in: AIP Conf Proc, AIP Publishing LLC AIP Publishing, 2020, p. 020072. https://doi.org/10.1063/5.0015799.
[67] Y.-H. Choi, C.-M. Kim, H.-S. Jeong, J.-H. Youn, Y.-H. Choi, C.-M. Kim, H.-S. Jeong, J.-H. Youn, Influence of Bed Temperature on Heat Shrinkage Shape Error in FDM Additive Manufacturing of the ABS-Engineering Plastic, World J. Eng. Technol. 4 (2016) 186–192, https://doi.org/10.4236/WJET.2016.43D022.
[68] H. Qu, W. Zhang, Z. Li, L. Hou, G. Li, J.Y. Fuh, W. Wu, Influence of Thermal Processing Conditions on Mechanical and Material Properties of 3D Printed Thin-Structures Using PEEK Material, Int. J. Precis. Eng. Manuf. 23 (2022) 689–699, https://doi.org/10.1007/S12541-022-00650-1/FIGURES/10.
[69] C. Basgul, T. Yu, D.W. MacDonald, R. Siskey, M. Marcolongo, S.M. Kurtz, Does annealing improve the interlayer adhesion and structural integrity of FFF 3D printed PEEK lumbar spinal cages? J. Mech. Behav. Biomed. Mater. 102 (2020) https://doi.org/10.1016/j.jmbbm.2019.103455.
[70] F. Léonard, S. Tammas-Williams, Metal FFF sintering shrinkage rate measurements by X-ray computed tomography, Nondestruct. Test. Eval. 37 (2022) 631–644, https://doi.org/10.1080/10589759.2022.2085702.
[71] B. Hu, X. Duan, Z. Xing, Z. Xu, C. Du, H. Zhou, R. Chen, B. Shan, Improved design of fused deposition modeling equipment for 3D printing of high-performance PEEK parts, Mech. Mater. 137 (2019), 103139, https://doi.org/10.1016/J.MECHMAT.2019.103139.
[72] T.G. Reynolds, Accelerated tests of environmental degradation in composite materials, Massachusetts Institute of Technology, 1998. https://dspace.mit.edu/handle/1721.1/28202 (accessed February 28, 2023).
[73] N.M. Barkoula, Environmental degradation of carbon nanotube hybrid aerospace composites, Solid Mech. Appl. 188 (2013) 337–376, https://doi.org/10.1007/978-94-007-4246-8_9.
[74] E. Kim, Y.J. Shin, S.H. Ahn, The effects of moisture and temperature on the mechanical properties of additive manufacturing components: Fused deposition modeling, Rapid Prototyp J. 22 (2016) 887–894, https://doi.org/10.1108/RPJ-08-2015-0095.
[75] A. de Nicola, A. Correa, G. Milano, P. la Manna, P. Musto, G. Mensitieri, G. Scherillo, Local Structure and Dynamics of Water Absorbed in Poly(ether imide): A Hydrogen Bonding Anatomy, J. Phys. Chem. B 121 (2017) 3162–3176, https://doi.org/10.1021/acs.jpcb.7b00992.
[76] M.A. Pop, C. Croitoru, T. Bedő, V. Geaman, I. Radomir, M. Coșnița, S.M. Zaharia, L.A. Chicoș, I. Miloșan, Structural changes during 3D printing of bioderived and synthetic thermoplastic materials, J. Appl. Polym. Sci. 136 (2019) 47382, https://doi.org/10.1002/APP.47382.
[77] L. Monson, M. Braunwarth, C.W. Extrand, Moisture absorption by various polyamides and their associated dimensional changes, J. Appl. Polym. Sci. 107 (2008) 355–363, https://doi.org/10.1002/app.27057.
[78] A.K. Ghosh, M. Dwivedi, Processability of Thermoplastic Composites, Processability of Polymeric, Composites (2020) 151–177, https://doi.org/10.1007/978-81-322-3933-8_6.
[79] T. Casalini, F. Rossi, A. Castrovinci, G. Perale, A Perspective on Polylactic Acid-Based Polymers Use for Nanoparticles Synthesis and Applications, Front. Bioeng. Biotechnol. 7 (2019) 259, https://doi.org/10.3389/FBIOE.2019.00259/BIBTEX.
[80] R. Wichniarek, A. Hamrol, W. Kuczko, F. Górski, M. Rogalewicz, ABS filament moisture compensation possibilities in the FDM process, CIRP J. Manuf. Sci. Technol. 35 (2021) 550–559, https://doi.org/10.1016/j.cirpj.2021.08.011.
[81] S.N.A.M. Halidi, J. Abdullah, Moisture effects on the ABS used for Fused Deposition Modeling rapid prototyping machine, SHUSER 2012–2012 IEEE Symposium on Humanities, Sci. Eng. Res. (2012) 839–843, https://doi.org/10.1109/SHUSER.2012.6268999.
[82] O. Urakawa, Polyetherimide, Encyclopedia of Polymeric Nanomaterials. (2014) 1–10, https://doi.org/10.1007/978-3-642-36199-9_411-1.
[83] C. Huang, X. Qian, R. Yang, Thermal conductivity of polymers and polymer nanocomposites, Mater. Sci. Eng. R. Rep. 132 (2018) 1–22, https://doi.org/10.1016/j.mser.2018.06.002.
[84] J.M. García, F.C. García, F. Serna, J.L. de la Peña, High-performance aromatic polyamides, Prog. Polym. Sci. 35 (2010) 623–686, https://doi.org/10.1016/J.PROGPOLYMSCI.2009.09.002.
[85] D. Nichetti, I. Manas-Zloczower, Influence of molecular parameters on material processability in extrusion processes, Polym. Eng. Sci. 39 (1999) 887–895, https://doi.org/10.1002/pen.11478.
[86] M.G.A. Vieira, M.A. Da Silva, L.O. Dos Santos, M.M. Beppu, Natural-based plasticizers and biopolymer films: A review, Eur. Polym. J. 47 (2011) 254–263, https://doi.org/10.1016/J.EURPOLYMJ.2010.12.011.
[87] I. Baek, O. Kwon, C.M. Lim, K.Y. Park, C.J. Bae, 3D PEEK Objects Fabricated by Fused Filament Fabrication (FFF), Materials 15 (2022) 1–26, https://doi.org/10.3390/ma15030898.
[88] S. Yuan, D. Strobbe, J.P. Kruth, P. Van Puyvelde, B. Van Der Bruggen, Super-hydrophobic 3D printed polysulfone membranes with a switchable wettability by self-assembled candle soot for efficient gravity-driven oil/water separation, J. Mater. Chem. A Mater. 5 (2017) 25401–25409, https://doi.org/10.1039/c7ta08836a.
[89] K.H. Tan, C.K. Chua, K.F. Leong, C.M. Cheah, P. Cheang, M.S. Abu Bakar, S. W. Cha, Scaffold development using selective laser sintering of polyetheretherketone-hydroxyapatite biocomposite blends, Biomaterials 24 (2003) 3115–3123, https://doi.org/10.1016/S0142-9612(03)00131-5.
[90] L. Pigliaru, M. Rinaldi, L. Ciccacci, A. Norman, T. Rohr, T. Ghidini, F. Nanni, 3D printing of high performance polymer-bonded PEEK-NdFeB magnetic composite materials, Funct. Compos. Mater. 1 (2020) 1–17, https://doi.org/10.1186/s42252-020-00006-w.
[91] C.V. Tigmeanu, L.C. Ardelean, L.C. Rusu, M.L. Negrutiu, Additive Manufactured Polymers in Dentistry, Current State-of-the-Art and Future Perspectives-A Review, Polymers (Basel) 14 (2022) 3658, https://doi.org/10.3390/polym14173658.
[92] L. Ding, W. Lu, J. Zhang, C. Yang, G. Wu, Preparation and performance evaluation of duotone 3d-printed polyetheretherketone as oral prosthetic materials: A proof-of-concept study, Polymers (Basel) 13 (2021) 1949, https://doi.org/10.3390/polym13121949.
[93] Y. Wu, Y. Cao, Y. Wu, D. Li, Neutron shielding performance of 3D-Printed boron carbide PEEK composites, Materials 13 (2020), 121058, https://doi.org/10.3390/ma13102314.
[94] Y. Wu, Y. Cao, Y. Wu, D. Li, Neutron shielding performance of 3D-Printed boron carbide PEEK composites, Materials 13 (2020) 2314, https://doi.org/10.3390/ma13102314.
[95] H. Jiang, P. Aihemaiti, W. Aiyiti, A. Kasimu, Study Of the compression behaviours of 3D-printed PEEK/CFR-PEEK sandwich composite structures, Virtual Phys. Prototyp. 17 (2022) 138–155, https://doi.org/10.1080/17452759.2021.2014636.
[96] Y. Wu, Y. Cao, Y. Wu, D. Li, Mechanical properties and gamma-ray shielding performance of 3d-printed poly-ether-ether-ketone/tungsten composites, Materials 13 (2020) 1–22, https://doi.org/10.3390/ma13204475.
[97] X. Liu, Z. Shan, J. Liu, H. Xia, X. Ao, A. Zou, S. Wu, Mechanical and electrical properties of additive manufactured high-performance continuous glass fiber reinforced PEEK composites, Compos. B Eng. 247 (2022), 110292, https://doi.org/10.1016/j.compositesb.2022.110292.
[98] J.J. Andrew, H. Alhashmi, A. Schiffer, S. Kumar, V.S. Deshpande, Energy absorption and self-sensing performance of 3D printed CF/PEEK cellular composites, Mater. Des. 208 (2021), 109863, https://doi.org/10.1016/j.matdes.2021.109863.
[99] A. Pulipaka, K.M. Gide, A. Beheshti, Z.S. Bagheri, Effect of 3D printing process parameters on surface and mechanical properties of FFF-printed PEEK, J. Manuf. Process. 85 (2023) 368–386, https://doi.org/10.1016/J.JMAPRO.2022.11.057.
[100] M. Rinaldi, F. Cecchini, L. Pigliaru, T. Ghidini, F. Lumaca, F. Nanni, Additive manufacturing of polyether ether ketone (Peek) for space applications: A nanosat polymeric structure, Polymers (Basel) 23 (2021) 1–16, https://doi.org/10.3390/polym13010011.
[101] C. Luo, Y. Liu, B. Peng, M. Chen, Z. Liu, Z. Li, H. Kuang, B. Gong, Z. Li, H. Sun, PEEK for Oral Applications: Recent Advances in Mechanical and Adhesive Properties, Polymers (Basel) 15 (2023) 386, https://doi.org/10.3390/polym15020386.
[102] Y. Shi, T. Deng, Y. Peng, Z. Qin, M. Ramalingam, Y. Pan, C. Chen, F. Zhao, L. Cheng, J. Liu, Effect of Surface Modification of PEEK Artificial Phalanx by 3D Printing on its Biological Activity, Coatings 13 (2023) 400, https://doi.org/10.3390/coatings13020400.
[103] L. Ren, W. Wu, L. Ren, Z. Song, Q. Liu, B. Li, Q. Wu, X. Zhou, 3D Printing of Auxetic Metamaterials with High-Temperature and Programmable Mechanical Properties, Adv Mater Technol. (2022) 2101546. https://doi.org/10.1002/admt.202101546.
[104] N. Vidakis, M. Petousis, N. Mountakis, E. Karapidakis, Box-Behnken modeling to quantify the impact of control parameters on the energy and tensile efficiency of PEEK in MEX 3D-printing, Heliyon 9 (2023) e18363.
[105] B. Hu, Z. Xing, W. Wu, X. Zhang, H. Zhou, C. Du, B. Shan, Enhancing the mechanical properties of SCF/PEEK composites in FDM via process-parameter optimization, High Perform Polym. 33 (2021) 914–923, https://doi.org/10.1177/09540083211003654.

[106] P. Wang, A. Pan, L. Xia, Y. Cao, H. Zhang, W. Wu, Effect of process parameters of fused deposition modeling on mechanical properties of poly-ether-ether-ketone and carbon fiber/poly-ether-ether-ketone, High Perform. Polym. 34 (2022) 337–351, https://doi.org/10.1177/09540083211067388.
[107] X. Ma, L. Wen, S. Wang, J. Xiao, W. Li, X. Hou, Inherent relationship between process parameters, crystallization and mechanical properties of continuous carbon fiber reinforced PEEK composites, Defence Technol. (2022), https://doi.org/10.1016/j.dt.2022.04.010.
[108] R. Wang, K.J. Cheng, R.C. Advincula, Q. Chen, On the thermal processing and mechanical properties of 3D-printed polyether ether ketone, MRS Commun. 9 (2019) 1046–1052, https://doi.org/10.1557/MRC.2019.86/FIGURES/4.
[109] Y. He, M. Shen, Q. Wang, T. Wang, X. Pei, Effects of FDM parameters and annealing on the mechanical and tribological properties of PEEK, Compos. Struct. 313 (2023), 116901, https://doi.org/10.1016/J.COMPSTRUCT.2023.116901.
[110] Q. Feng, W. Maier, H.C. Möhring, Application of machine learning to optimize process parameters in fused deposition modeling of PEEK material, Procedia CIRP 107 (2022) 1–8, https://doi.org/10.1016/J.PROCIR.2022.04.001.
[111] M. Garcia-Leiner, B. Streifel, C. Başgül, D.W. MacDonald, S.M. Kurtz, Characterization of polyaryletherketone (PAEK) filaments and printed parts produced by extrusion-based additive manufacturing, Polym. Int. 70 (2021) 1128–1136, https://doi.org/10.1002/PI.6231.
[112] K.C.H. Gardner, B.S. Hsiao, R.R. Matheson, B.A. Wood, Structure, crystallization and morphology of poly (aryl ether ketone ketone), Polymer (Guildf) 33 (1992) 2483–2495, https://doi.org/10.1016/0032-3861(92)91128-O.
[113] P. Chen, H. Wang, J. Su, Y. Tian, S. Wen, B. Su, C. Yang, B. Chen, K. Zhou, C. Yan, Y. Shi, P. Chen, H. Wang, J. Su, S. Wen, B. Su, C. Yan, Y. Shi, Y. Tian, K. Zhou, C. Yang, Recent Advances on High-Performance Polyaryletherketone Materials for Additive Manufacturing, Adv. Mater. 34 (2022) 2200750, https://doi.org/10.1002/ADMA.202200750.
[114] W. Wang, J.M. Schultz, B.S. Hsiao, Dynamic study of crystallization- and melting-induced phase separation in PEEK/PEKK blends, Macromolecules 30 (1997) 4544–4550, https://doi.org/10.1021/MA970092L/ASSET/IMAGES/LARGE/MA970092LF00008.JPEG.
[115] R. Davies, N. Yi, P. McCutchion, O. Ghita, Mechanical property variance amongst vertical fused filament fabricated specimens via four different printing methods, Polym. Int. 70 (2021) 1073–1079, https://doi.org/10.1002/PI.6172.
[116] B.W. Kaplun, R. Zhou, K.W. Jones, M.L. Dunn, C.M. Yakacki, Influence of orientation on mechanical properties for high-performance fused filament fabricated ultem 9085 and electro-statically dissipative polyetherketoneketone, Addit. Manuf. 36 (2020), 101527, https://doi.org/10.1016/J.ADDMA.2020.101527.
[117] A. Scott, Exclusive: Boeing's space taxis to use more than 600 3D-printed parts | Reuters, Reuters. (2017). https://www.reuters.com/article/us-boeing-space-exclusive-idUSKBN15I1HW (accessed March 29, 2023).
[118] L. Prasanthi Nori, S.S. Manikiran, An outlook on regulatory aspects of 3D printing in pharmaceutical and medical sectors, Curr. Trends Pharm. Pharma. Chem. 4 (2022) 98–108. https://doi.org/10.18231/J.CTPPC.2022.017.
[119] G.R. Cobb, T.E. Shelton, C.R. Hartsfield, R.A. Kemnitz, Effects of carbon nanotube filler on mechanical and electrical properties of fused filament fabricated polyetherketoneketone, AIAA Scitech 2021 Forum. (2021) 1–11. https://doi.org/10.2514/6.2021-0168.
[120] K. Rashed, A. Kafi, R. Simons, S. Bateman, Optimization of material extrusion additive manufacturing process parameters for polyether ketone ketone (PEKK), Int. J. Adv. Manuf. Technol. (2023) 1–25, https://doi.org/10.1007/S00170-023-11167-W/TABLES/8.
[121] A. Lepoivre, A. Levy, N. Boyard, V. Gaudefroy, V. Sobotka, Coalescence in fused filament fabrication process: Thermo-dependent characterization of high-performance polymer properties, Polym. Test. 98 (2021), 107096, https://doi.org/10.1016/j.polymertesting.2021.107096.
[122] Z.C. Kennedy, J.F. Christ, M.D. Fenn, L. Zhong, W. Chouyyok, A.M. Arnold, A. C. Denny, A.M. Albrecht, J.A. Silverstein, R.L. Erikson, J. Chun, Mica filled polyetherketoneketones for material extrusion 3D printing, Addit. Manuf. 49 (2022), 102492, https://doi.org/10.1016/J.ADDMA.2021.102492.
[123] E.B. Caldona, J.R.C. Dizon, R.A. Viers, V.J. Garcia, Z.J. Smith, R.C. Advincula, Additively manufactured high-performance polymeric materials and their potential use in the oil and gas industry, MRS Commun. 11 (2021) 701–715, https://doi.org/10.1557/S43579-021-00134-9/FIGURES/7.
[124] L.W. McKeen, High-Temperature Polymers, William Andrew Publishing (2009), https://doi.org/10.1016/B978-0-8155-1585-2.50012-1.
[125] M.M. Garmabi, P. Shahi, J. Tjong, M. Sain, 3D printing of polyphenylene sulfide for functional lightweight automotive component manufacturing through enhancing interlayer bonding, Addit. Manuf. 56 (2022), 102780, https://doi.org/10.1016/j.addma.2022.102780.
[126] L. Martinez, D. Palessonga, P. Roquefort, A. Chevalier, A. Maalouf, J. Ville, V. Laur, Development of a high temperature printable composite for microwave absorption applications, AIMS Mater. Sci. 8 (2021) 739–747, https://doi.org/10.3934/matersci.2021044.
[127] M.Q. Ansari, M.J. Bortner, D.G. Baird, Generation of Polyphenylene Sulfide Reinforced with a Thermotropic Liquid Crystalline Polymer for Application in Fused Filament Fabrication, Addit. Manuf. 29 (2019), 100814, https://doi.org/10.1016/J.ADDMA.2019.100814.
[128] M. Parker, N. Ezeokeke, R. Matsuzaki, D. Arola, Strength and its variability in 3D printing of polymer composites with continuous fibers, Mater. Des. 225 (2023), 111505, https://doi.org/10.1016/J.MATDES.2022.111505.
[129] J. Retolaza, K. Gondra, R. Ansola, A. Allue, Mechanical research to optimize parameter selection for PPS material processed by FDM, Mater. Manuf. Process. 37 (2022) 1332–1338, https://doi.org/10.1080/10426914.2022.2072875.
[130] A. El Magri, K. El Mabrouk, S. Vaudreuil, M. Ebn Touhami, Experimental investigation and optimization of printing parameters of 3D printed polyphenylene sulfide through response surface methodology, J. Appl. Polym. Sci. 138 (2021) 49625, https://doi.org/10.1002/APP.49625.
[131] E.R. Fitzharris, I. Watt, D.W. Rosen, M.L. Shofner, Interlayer bonding improvement of material extrusion parts with polyphenylene sulfide using the Taguchi method, Addit. Manuf. 24 (2018) 287–297, https://doi.org/10.1016/j.addma.2018.10.003.
[132] P. Geng, J. Zhao, W. Wu, Y. Wang, B. Wang, S. Wang, G. Li, Effect of thermal processing and heat treatment condition on 3D printing PPS properties, Polym. (Basel) 10 (2018) 875, https://doi.org/10.3390/polym10080875.
[133] X. Xu, H. Wang, S. Zhang, X. Mei, B. Ying, R. Li, Y. Qin, ECM-inspired 3D printed polyetherimide scaffold with Arg-Gly-Asp peptides for the improvement of bioactivity and osteogenic differentiation of osteoblasts, Mater. Today Commun. 30 (2022), 103166, https://doi.org/10.1016/J.MTCOMM.2022.103166.
[134] M. Rouway, M. Tarfaoui, N. Chakhchaoui, L. El, H. Omari, F. Fraija, O. Cherkaoui, Additive Manufacturing and Composite Materials for Marine Energy: Case of Tidal Turbine, 3D Print Addit Manuf. (2021). https://doi.org/10.1089/3DP.2021.0194.
[135] Stratasys, ULTEM^{TM} 1010 resin - FDM 3D Printing Material, (n.d.). https://www.stratasys.com/en/materials/materials-catalog/fdm-materials/ultem-1010/ (accessed March 30, 2023).
[136] Stratasys, ULTEM 9085 resin: High Performance Thermoplastic, (n.d.). https://www.stratasys.com/en/materials/materials-catalog/fdm-materials/ultem-9085/ (accessed March 30, 2023).
[137] A.W. Gebisa, H.G. Lemu, Influence of 3D printing FDM process parameters on tensile property of ultem 9085, in: Procedia Manuf, Elsevier B.V., 2019: pp. 331–338. https://doi.org/10.1016/j.promfg.2019.02.047.
[138] S.-E. Ouassil, Anouar, E. Magri, Hamid, R. Vanaei, S. Vaudreuil, H.R. Vanaei, L. De Vinci, Investigating the effect of printing conditions and annealing on the porosity and tensile behavior of 3D-printed polyetherimide material in Z-direction, J. Appl. Polym. Sci. 140 (2023) e53353.
[139] M. Yilmaz, N.F. Yilmaz, M.F. Kalkan, Rheology, Crystallinity, and Mechanical Investigation of Interlayer Adhesion Strength by Thermal Annealing of Polyetherimide (PEI/ULTEM 1010) Parts Produced by 3D Printing, J. Mater. Eng. Perform. 31 (2022) 9900–9909, https://doi.org/10.1007/S11665-022-07049-Z/TABLES/2.
[140] P. Han, A. Tofangchi, A. Deshpande, S. Zhang, K. Hsu, An approach to improve interface healing in FFF-3D printed Ultem 1010 using laser pre-deposition heating, in: Procedia Manuf, Elsevier, 2019: pp. 672–677. https://doi.org/10.1016/j.promfg.2019.06.195.
[141] P. Han, S. Zhang, A. Tofangchi, K. Hsu, Relaxation of residual stress in fused filament fabrication part with in-process laser heating, in: Procedia Manuf, Elsevier B.V., 2021, pp. 466–471. https://doi.org/10.1016/j.promfg.2021.06.080.
[142] H. Wu, M. Sulkis, J. Driver, A. Saade-Castillo, A. Thompson, J.H. Koo, Multi-functional ULTEMTM1010 composite filaments for additive manufacturing using Fused Filament Fabrication (FFF), Addit. Manuf. 24 (2018) 298–306, https://doi.org/10.1016/j.addma.2018.10.014.
[143] Q. Chen, Y.Y. Zhang, P. Huang, Y.Q. Li, S.Y. Fu, Improved bond strength, reduced porosity and enhanced mechanical properties of 3D-printed polyetherimide composites by carbon nanotubes, Compos. Commun. 30 (2022), 101083, https://doi.org/10.1016/j.coco.2022.101083.
[144] M. Karabal, R. Yuksel, F. Kayginok, A. Yildiz, H. Cebeci, Embedded Piezoresistive Sensors Printed by FFF for Aerospace Applications, Mater. Additive Manuf. (2023), https://doi.org/10.2514/6.2023-0318.
[145] S.W. Paek, S. Balasubramanian, D. Stupples, Composites Additive Manufacturing for Space Applications: A Review, Materials. 15 (2022) 4387–4398, https://doi.org/10.3390/ma15134709.
[146] A. Abbott, T. Gibson, G.P. Tandon, L. Hu, R. Avakian, J. Baur, H. Koerner, Melt extrusion and additive manufacturing of a thermosetting polyimide, Addit Manuf. 37 (2021), 101636, https://doi.org/10.1016/j.addma.2020.101636.
[147] X. Feng, J. Liu, Thermoplastic Polyimide (TPI), in: High Performance Polymers and Their Nanocomposites, John Wiley & Sons, Inc., 2018: pp. 149–219. https://doi.org/10.1002/9781119363910.CH6.
[148] W. Wu, W. Ye, P. Geng, Y. Wang, G. Li, X. Hu, J. Zhao, 3D printing of thermoplastic PI and interlayer bonding evaluation, Mater Lett. 229 (2018) 206–209, https://doi.org/10.1016/J.MATLET.2018.07.020.
[149] W. Ye, G. Lin, W. Wu, P. Geng, X. Hu, Z. Gao, J. Zhao, Separated 3D printing of continuous carbon fiber reinforced thermoplastic polyimide, Compos. Part A Appl. Sci. Manuf. 121 (2019) 457–464, https://doi.org/10.1016/J.COMPOSITESA.2019.04.002.
[150] V.R. Sastri, Chapter 8 - High-Temperature Engineering Thermoplastics: Polysulfones, Polyimides, Polysulfides, Polyketones, Liquid Crystalline Polymers, and Fluoropolymers, in: Plastics Design Library, William Andrew Publishing, 2010: pp. 175–215. https://doi.org/10.1016/B978-0-8155-2027-6.10008-X.
[151] M.T. DeMeuse, Polysulfones as a reinforcement in high temperature polymer blends, High Temperature Polymer Blends (2014) 165–173, https://doi.org/10.1533/9780857099013.165.
[152] L.M. Schönhoff, F. Mayinger, M. Eichberger, E. Reznikova, B. Stawarczyk, 3D printing of dental restorations: Mechanical properties of thermoplastic polymer materials, J. Mech. Behav. Biomed. Mater. 119 (2021), 104544, https://doi.org/10.1016/J.JMBBM.2021.104544.

[153] L.M. Schönhoff, F. Mayinger, M. Eichberger, A. Lösch, E. Reznikova, B. Stawarczyk, Three-dimensionally printed and milled polyphenylene sulfone materials in dentistry: Tensile bond strength to veneering composite resin and surface properties after different pretreatments, J. Prosthet Dent. 128 (2022) 93–99, https://doi.org/10.1016/J.PROSDENT.2020.12.042.
[154] C. Ajinjeru, V. Kishore, X. Chen, J. Lindahl, Z. Sudbury, A.A. Hassen, V. Kunc, B. Post, L. Love, C. Duty, The Influence of Rheology on Melt Processing Conditions of Amorphous Thermoplastics for Big Area Additive Manufacturing (BAAM), in: Solid Freeform Fabrication 2016: Proceedings of the 26th Annual International Solid Freeform Fabrication Symposium – An Additive Manufacturing Conference, 2016.
[155] M. Ramesh, M. Muthukrishnan, Biodegradable polymer blends and composites for food-packaging applications, in: Biodegradable Polymers, Blends and Composites, Woodhead Publishing, 2021, pp. 693–716. https://doi.org/10.1016/B978-0-12-823791-5.00004-1.
[156] Y. Qin, Applications of advanced technologies in the development of functional medical textile materials, in: Medical Textile Materials, Woodhead Publishing, 2016, pp. 55–70. https://doi.org/10.1016/b978-0-08-100618-4.00005-4.
[157] A. Dorigato, Recycling of polymer blends, Advanced Industrial and Engineering Polymer, Research 4 (2021) 53–69, https://doi.org/10.1016/j.aiepr.2021.02.005.
[158] A.J. Ryan, Polymer science: Designer polymer blends, Nat. Mater. 1 (2002) 8–10, https://doi.org/10.1038/nmat720.
[159] Z. Horák, I. Fortelný, J. Kolařík, D. Hlavatá, A. Sikora, Polymer Blends, Kirk-Othmer Encycl. Chem. Technol. (2005), https://doi.org/10.1002/0471238961.1615122511051911.A01.PUB2.
[160] M. Pracella, Crystallization of Polymer Blends, Handbook of Polymer Crystallization. (2013) 287–325. https://doi.org/10.1002/9781118541838.CH10.
[161] A. Arzak, J.I. Eguiazábal, J. Nazábal, Biphasic compatible blends from injection-molded poly (ether ether ketone)/polysulfone, J. Appl. Polym. Sci. 65 (1997) 1503–1510, https://doi.org/10.1002/(SICI)1097-4628(19970822)65:8<1503::AID-APP7>3.0.CO;2-K.
[162] A. Tewatia, J. Hendrix, T. Nosker, J. Lynch, High shear melt-processing of polyetheretherketone enhanced polysulfone immiscible polymer blends, in: 2018 Society of Plastics Engineers Annual Technical Conference, Orlando, 2018. https://www.researchwithrutgers.com/en/publications/high-shear-melt-processing-of-polyetheretherketone-enhanced-polys (accessed March 14, 2023).
[163] T. Hoffmann, D. Pospiech, L. Häussler, P. Pötschke, U. Reuter, P. Werner, J.K. W. Sandler, M. Döring, V. Altstädt, Properties of segmented block copolymers in PEEK/PSU blends, High Perform. Polym. 20 (2008) 601–614, https://doi.org/10.1177/0954008307082176.
[164] T.M. Malik, Thermal and mechanical characterization of partially miscible blends of poly(ether ether ketone) and polyethersulfone, J. Appl. Polym. Sci. 46 (1992) 303–310, https://doi.org/10.1002/app.1992.070460211.
[165] B. Nandan, L.D. Kandpal, G.N. Mathur, Polyetherether ketone/polyarylethersulfone blends: Thermal and compatibility aspects, J. Polym. Sci. B Polym. Phys. 40 (2002) 1407–1424, https://doi.org/10.1002/polb.10199.
[166] Z. Hong, W.D. Yang, Y.S. Wei, W. Bin Yang, X.Q. Yu, X.D. Cao, Studies on proton conductivity and methanol permeability of poly(ether sulfone)/sulfonated poly (ether ether ketone) blend membranes, in: Materials Research Society Symposium Proceedings, 2008, pp. 33–39. https://doi.org/10.1557/proc-1098-hh03-12.
[167] Z. Wu, Y. Zheng, X. Yu, T. Nakamura, R. Yosomiya, Thermal and viscoelastic behavior of polyetheretherketone/polyethersulfone blends, Die Angewandte Makromolekulare Chemie. 171 (1989) 119–130, https://doi.org/10.1002/apmc.1989.051710109.
[168] Z. Ni, The preparation, compatibility and structure of PEEK–PES blends, Polym. Adv. Technol. 5 (1994) 612–614, https://doi.org/10.1002/pat.1994.220050927.
[169] B. Nandan, L.D. Kandpal, G.N. Mathur, Poly(ether ether ketone)/Poly(aryl ether sulfone) Blends: Melt Rheological Behavior, J. Polym. Sci. B Polym. Phys. 42 (2004) 1548–1563, https://doi.org/10.1002/polb.20039.
[170] A. Korycki, C. Garnier, A. Abadie, V. Nassiet, C.T. Sultan, F. Chabert, Poly (etheretherketone)/poly(ethersulfone) blends with phenolphthalein: Miscibility, thermomechanical properties, crystallization and morphology, Polymers (Basel). 13 (2021), https://doi.org/10.3390/polym13091466.
[171] M. Shibata, Z. Fang, R. Yosomiya, A study of blends of poly(ether ether ketone ketone) and poly(ether sulphone): Effect of the addition of poly (ether ether ketone) oligomer, Polym. Polym. Compos. 4 (1996) 483–488.
[172] A. Arzak, J.I. Eguiazábal, J. Nazábal, Compatibility in immiscible poly(ether ether ketone)/poly(ether sulfone) blends, J. Appl. Polym. Sci. 58 (1995) 653–661, https://doi.org/10.1002/app.1995.070580320.
[173] S. Mandal, S. Alam, Studies on the mechanical, thermal, and morphological properties of poly(ether ether ketone)/poly(ether sulfone)/barium titanate nanocomposites: Correlation of experimental results with theoretical predictive models, J. Appl. Polym. Sci. 126 (2012) 724–733, https://doi.org/10.1002/app.36735.
[174] G. Crevecoeur, G. Groeninckx, Binary Blends of Poly(ether ether ketone) and Poly (ether imide). Miscibility, Crystallization Behavior, and Semicrystalline Morphology, Macromolecules 24 (1991) 1190–1195, https://doi.org/10.1021/ma00005a034.
[175] D.A. Ivanov, A.M. Jonas, Vitrification/ Devitrification Phenomena during Isothermal and Nonisothermal Crystallization of Poly (aryl-ether-ether-ketone) (PEEK) and PEEK /Poly(ether-imide) Blends, Polym. Phys. 36 (1998) 919–930, https://doi.org/10.1002/(SICI)1099-0488(19980415)36:5.
[176] M. Rosa, L. Grassia, A. D'Amore, C. Carotenuto, M. Minale, Rheology and mechanics of polyether(ether)ketone - Polyetherimide blends for composites in aeronautics, AIP Conference Proceedings 1736 (2016), https://doi.org/10.1063/1.4949752.
[177] B.H. Stuart, Tribological studies of poly(ether ether ketone) blends, Tribol. Int. 31 (1998) 647–651, https://doi.org/10.1016/S0301-679X(98)00090-5.
[178] R. Ramani, S. Alam, Composition optimization of PEEK/PEI blend using model-free kinetics analysis, Thermochim. Acta 511 (2010) 179–188, https://doi.org/10.1016/j.tca.2010.08.012.
[179] P.T. Rajagopalan, L.D. Kandpal, A.K. Tewary, R.P. Singh, K.N. Pandey, G. N. Mathur, Thermal behaviour of polyetherimide PEEK blends, J. Therm. Anal. 49 (1997) 143–147, https://doi.org/10.1007/bf01987432.
[180] R. Ramani, S. Alam, Influence of an organophosphonite antioxidant on the thermal behavior of PEEK/PEI blend, Thermochim. Acta 550 (2012) 33–41, https://doi.org/10.1016/j.tca.2012.09.023.
[181] A.M. Díez-Pascual, A.L. Díez-Vicente, Nano-TiO2 reinforced PEEK/PEI blends as biomaterials for load-bearing implant applications, ACS Appl. Mater. Interfaces 7 (2015) 5561–5573, https://doi.org/10.1021/acsami.5b00210.
[182] A. Ahamad, P. Kumar, Mechanical and thermal performance of PEEK/PEI blend matrix reinforced with surface modified halloysite nanotubes, J. Thermoplast. Compos. Mater. (2021), https://doi.org/10.1177/08927057211028629.
[183] B. Nandan, B. Lal, K.N. Pandey, S. Alam, L.D. Kandpal, G.N. Mathur, Studies on high performance PEEK based alumina composites, J. Polym. Mater. 18 (2001) 135–140.
[184] R.E.S. Bretas, D.G. Baird, Miscibility and mechanical properties of poly(ether imide)/poly(ether ether ketone)/liquid crystalline polymer ternary blends, Polymer (Guildf) 33 (1992) 5233–5244, https://doi.org/10.1016/0032-3861(92)90806-8.
[185] R.E.S. Bretas, D. Collias, D.G. Baird, Dynamic rheological properties of polyetherimide/polyetheretherketone/liquid crystalline polymer ternary blends, Polym. Eng. Sci. 34 (1994) 1492–1496, https://doi.org/10.1002/pen.760341909.
[186] E.M. Woo, Y.C. Tseng, Analysis and characterization of unusual ternary polymer miscibility in poly(ether diphenyl ether ketone), poly(ether ether ketone), and poly(ether imide), Macromol. Chem. Phys. 201 (2000) 1877–1886, https://doi.org/10.1002/1521-3935(20000901)201:14<1877::AID-MACP1877>3.0.CO;2-C.
[187] C.B. Crawford, B. Quinn, Physiochemical properties and degradation, Microplastic Pollutants (2017) 57–100, https://doi.org/10.1016/B978-0-12-809406-8.00004-9.
[188] G. Primc, Recent advances in surface activation of polytetrafluoroethylene (PTFE) by gaseous plasma treatments, Polymers (Basel) 12 (2020) 1–7, https://doi.org/10.3390/polym12102295.
[189] W. Hufenbach, K. Kunze, J. Bijwe, Sliding wear behaviour of PEEK-PTFE blends, J. Synth. Lubr. 20 (2003) 227–240, https://doi.org/10.1002/jsl.3000200305.
[190] C. Chan, A. Nixon, S. Venkatraman, Effects of the low-surface-energy component on the viscosity of poly(ether ether ketone) and polytetrafluoroethylene blends, J. Rheol. (N Y N Y) 36 (1992) 807–820, https://doi.org/10.1122/1.550318.
[191] X. Qiu, C. Fu, A. Gu, Y. Gao, X. Wang, Z. Yu, Preparation of high-performance PEEK anti-wear blends with melt-processable PTFE, High Perform. Polym. 32 (2020) 645–654, https://doi.org/10.1177/0954008319893741.
[192] A. Frick, D. Sich, G. Heinrich, C. Stern, M. Schlipf, Classification of New Melt-Processable PTFE: Comparison of Emulsion- and Suspension-Polymerized Materials, Macromol. Mater. Eng. 297 (2012) 329–341, https://doi.org/10.1002/MAME.201100149.
[193] A. Frick, D. Sich, G. Heinrich, D. Lehmann, U. Gohs, C. Stern, Properties of melt processable PTFE/PEEK blends: The effect of reactive compatibilization using electron beam irradiated melt processable PTFE, J. Appl. Polym. Sci. 128 (2013) 1815–1827, https://doi.org/10.1002/app.38337.
[194] X.D. Peng, H.Y. Ma, Y. Lei, Tribological behaviors of polyetherether ketone composites filled with nanometer Al2O3 and polytetrafluoroethylene, Shiyou Daxue Xuebao/Journal of the University of Petroleum China. 28 (2004) 68-70+74.
[195] X. Peng, Q. Zeng, H. Ma, Y. Lei, Study on the load and time-dependent of the frictional behavior of PEEK composites filled with nano-Al2O3 and PTFE, Run Hua Yu Mi Feng/Lubrication Engineering (2005) 56–58.
[196] X. Teng, L. Wen, Y. Lv, W. Tang, X. Zhao, C. Chen, Effects of potassium titanate whisker and glass fiber on tribological and mechanical properties of PTFE/PEEK blend, High Perform. Polym. 30 (2018) 752–764, https://doi.org/10.1177/0954008317723444.
[197] T.S. Frank Gladson, R. Ramesh, C. Kavitha, Experimental investigation of mechanical, tribological and dielectric properties of alumina nano wire-reinforced PEEK/PTFE composites, Mater. Res. Express. 6 (2019), 115327, https://doi.org/10.1088/2053-1591/ab491d.
[198] S.M. Santos, S. Qu, S.S. Wang, Elevated-temperature thermal conductivity for PEEK-matrix composite with carbon fibers, graphite flakes and PTFE, in: Proceedings of the American Society for Composites - 35th Technical Conference, ASC 2020, DEStech Publications, 2020, pp. 520–538. https://doi.org/10.12783/asc35/34877.
[199] A. Miyase, S. Qu, K.H. Lo, S.S. Wang, Elevated-Temperature Thermal Expansion of PTFE/PEEK Matrix Composite with Random-Oriented Short Carbon Fibers and Graphite Flakes, Journal of Engineering Materials and Technology, Trans. ASME 142 (2020), https://doi.org/10.1115/1.4045158.
[200] Z. Jin, Z. Yao, Y. Sun, H. Shen, Loading capacity of PEEK blends in terms of wear rate and temperature, Wear 496–497 (2022), 204306, https://doi.org/10.1016/j.wear.2022.204306.
[201] R.K. Krishnaswamy, D.S. Kalika, Phase behavior, crystallization, and morphology of poly(Ether Ether Ketone)/polyarylate blends, Polym. Eng. Sci. 36 (1996) 786–796, https://doi.org/10.1002/pen.10466.

[202] C. Gao, S. Zhang, X. Li, S. Zhu, Z. Jiang, Synthesis of poly(ether ether ketone)-block-polyimide copolymer and its compatibilization for poly(ether ether ketone)/thermoplastic polyimide blends, Polymer (Guildf) 55 (2014) 119–125, https://doi.org/10.1016/j.polymer.2013.11.022.
[203] C. Gao, S. Zhang, Y. Lin, F. Li, S. Guan, Z. Jiang, High-performance conductive materials based on the selective location of carbon black in poly(ether ether ketone)/polyimide matrix, Compos. B Eng. 79 (2015) 124–131, https://doi.org/10.1016/j.compositesb.2015.03.047.
[204] S. Park, K. (Kelvin) Fu, Polymer-based filament feedstock for additive manufacturing, Compos. Sci. Technol. 213 (2021), 108876, https://doi.org/10.1016/J.COMPSCITECH.2021.108876.
[205] B.S. Hsiao, B.B. Sauer, Glass transition, crystallization, and morphology relationships in miscible poly(aryl ether ketones) and poly(ether imide) blends, J. Polym. Sci. B Polym. Phys. 31 (1993) 901–915, https://doi.org/10.1002/polb.1993.090310801.
[206] S. Dominguez, C. Derail, F. Léonardi, J. Pascal, B. Brulé, Study of the thermal properties of miscible blends between poly(ether ketone ketone) (PEKK) and polyimide, Eur. Polym. J. 62 (2015) 179–185, https://doi.org/10.1016/j.eurpolymj.2014.10.024.
[207] B.B. Sauer, B.S. Hsiao, Miscibility of three different poly(aryl ether ketones) with a high melting thermoplastic polyimide, Polymer (Guildf) 34 (1993) 3315–3318, https://doi.org/10.1016/0032-3861(93)90409-4.
[208] B.B. Sauer, B.S. Hsiao, K.L. Faron, Miscibility and phase properties of poly(aryl ether ketone)s with three high temperature all-aromatic thermoplastic polyimides, Polymer (Guildf) 37 (1996) 445–453, https://doi.org/10.1016/0032-3861(96)82914-4.
[209] A. Mehta, A.I. Isayev, The dynamic properties, temperature transitions, and thermal stability of poly (etherether ketone)-thermotropic liquid crystalline polymer blends, Polym. Eng. Sci. 31 (1991) 963–970, https://doi.org/10.1002/pen.760311306.
[210] Y. Son, Y.S. Chun, R.A. Weiss, Improvement of the processability of poly(ether ketone ketone) by the addition of a thermotropic liquid crystalline polymer, Polym. Eng. Sci. 44 (2004) 541–547, https://doi.org/10.1002/pen.20048.
[211] I. Blanco, G. Cicala, G. Ognibene, M. Rapisarda, A. Recca, Thermal properties of polyetherimide/polycarbonate blends for advanced applications, Polym. Degrad. Stab. 154 (2018) 234–238, https://doi.org/10.1016/j.polymdegradstab.2018.06.011.
[212] G. Cicala, G. Ognibene, S. Portuesi, I. Blanco, M. Rapisarda, E. Pergolizzi, G. Recca, Comparison of Ultem 9085 used in fused deposition modelling (FDM) with polytherimide blends, Materials. 11 (2018), https://doi.org/10.3390/ma11020285.
[213] Y.S. Chun, H.S. Lee, W.N. Kim, T.S. Oh, Thermal properties and morphology of blends of poly(ether imide) and polycarbonate, Polym. Eng. Sci. 36 (1996) 2694–2702, https://doi.org/10.1002/PEN.10668.
[214] M. Zhang, P. Choi, U. Sundararaj, Molecular dynamics and thermal analysis study of anomalous thermodynamic behavior of poly (ether imide)/polycarbonate blends, Polymer (Guildf) 44 (2003) 1979–1986, https://doi.org/10.1016/S0032-3861(03)00054-5.
[215] K.-Y. Choi, S.-G. Lee, J.H. Lee, J. Liu, Morphology and dynamic mechanical properties of nylon 66/ poly(ether imide) blends, Polym. Eng. Sci. 35 (1995) 1643–1651, https://doi.org/10.1002/PEN.760352011.
[216] J. Ramiro, J.I. Eguiazábal, J. Nazábal, Structure and mechanical properties of blends of poly(ether imide) and an amorphous polyamide, Eur. Polym. J. 42 (2006) 458–467, https://doi.org/10.1016/j.eurpolymj.2005.07.002.
[217] J. Ramiro, J.I. Eguiazábal, J. Nazábal, Compatibilized poly(ether imide)/amorphous polyamide blends by means of poly(ethylene terephthalate) addition, Polym. Eng. Sci. 46 (2006) 1292–1298, https://doi.org/10.1002/pen.20575.
[218] M. Vásquez-Rendón, M.L. Álvarez-Láinez, Tailoring the mechanical, thermal, and flammability properties of high-performance PEI/PBT blends exhibiting dual-phase continuity, Polymer (Guildf) 154 (2018) 241–252, https://doi.org/10.1016/j.polymer.2018.09.012.
[219] F.J. Vallejo, J.I. Eguiazábal, J. Nazábal, Solid state features and mechanical properties of PEI/PBT blends, J. Appl. Polym. Sci. 80 (2001) 885–892, https://doi.org/10.1002/1097-4628(20010509)80:6<885::AID-APP1166>3.0.CO;2-D.
[220] M. Vásquez-Rendón, M.L. Álvarez-Láinez, PTFE as a toughness modifier of high-performance PEI/PBT blends: Morphology control during melt processing, Polym. Adv. Technol. 32 (2021) 714–724, https://doi.org/10.1002/pat.5124.
[221] M.R. Nobile, D. Acierno, L. Incarnato, L. Nicolais, The rheological behavior of a polyetherimide and of its blends with a thermotropic copolyester, J. Rheol. (N Y N Y) 34 (1990) 1181–1197, https://doi.org/10.1122/1.550080.
[222] S.S. Bafna, T. Sun, D.G. Baird, The role of partial miscibility on the properties of blends of a polyetherimide and two liquid crystalline polymers, Polymer (Guildf) 34 (1993) 708–715, https://doi.org/10.1016/0032-3861(93)90352-B.
[223] S. Bose, N. Pramanik, C.K. Das, A. Ranjan, A.K. Saxena, Synthesis and effect of polyphosphazenes on the thermal, mechanical and morphological properties of poly(etherimide)/thermotropic liquid crystalline polymer blend, Mater. Des. 31 (2010) 1148–1155, https://doi.org/10.1016/J.MATDES.2009.09.036.
[224] G.C. Nayak, R. Rajasekar, C.K. Das, Effect of SiC coated MWCNTs on the thermal and mechanical properties of PEI/LCP blend, Compos. Part A Appl. Sci. Manuf. 41 (2010) 1662–1667, https://doi.org/10.1016/J.COMPOSITESA.2010.08.003.
[225] G. Hatui, C.K. Das, Modification of CNT and its effect on thermo mechanical, morphological as well as rheological properties of Polyether Imide (PEI)/Liquid Crystalline Polymer (LCP) blend system, J. Polym. Res. 20 (2013) 1–12, https://doi.org/10.1007/S10965-013-0077-9/FIGURES/11.
[226] G.C. Nayak, S. Sahoo, S. Das, G. Karthikeyan, C.K. Das, A.K. Saxena, A. Ranjan, Compatibilization of polyetherimide/liquid crystalline polymer blend using modified multiwalled carbon nanotubes and polyphosphazene as compatibilizers, J. Appl. Polym. Sci. 124 (2012) 629–637, https://doi.org/10.1002/app.35005.
[227] Y. Seo, S.M. Hong, S.S. Hwang, T.S. Park, K.U. Kim, S. Lee, J. Lee, Compatibilizing effect of a poly(ester imide) on the properties of the blends of poly(ether imide) and a thermotropic liquid crystalline polymer: 1. Compatibilizer synthesis and thermal and rheological properties of the in situ composite system, Polymer (Guildf) 36 (1995) 515–523, https://doi.org/10.1016/0032-3861(95)91560-T.
[228] A. Granado, J.I. Eguiazábal, J. Nazábal, Processability, structure and mechanical properties of poly(ether imide)/amorphous copolyester blends, Macromol. Mater. Eng. 295 (2010) 476–483, https://doi.org/10.1002/mame.200900378.
[229] J. Ramiro, J.I. Egulazábal, J. Nazábal, New miscible poly(ether imide)/ poly (phenyl sulfone) blends, Macromol. Mater. Eng. 291 (2006) 707–713, https://doi.org/10.1002/mame.200500429.
[230] I. Blanco, M. Rapisarda, S. Portuesi, G. Ognibene, G. Cicala, Thermal behavior of PEI/PETG blends for the application in fused deposition modelling (FDM), in: AIP Conf Proc, American Institute of Physics Inc., 2018. https://doi.org/10.1063/1.5046043.
[231] T. Sugama, Polytetrafluoroethylene-Blended Polyphenylenesulphide Coatings for Mitigating Corrosion of Steel in Geothermal Environments, Polym. Polym. Compos. 6 (1998) 373–385, https://doi.org/10.1177/147823919800600602.
[232] Y. Shi, S.T. Zhou, Z.G. Heng, M. Liang, Y. Wu, Y. Chen, H.W. Zou, Interlocking Structure Formed by Multiscale Carbon Fiber-Polytetrafluoroethylene Fiber Hybrid Significantly Enhances the Friction and Wear Properties of Polyphenylene Sulfide Based Composites, Ind. Eng. Chem. Res. 58 (2019) 16541–16551, https://doi.org/10.1021/acs.iecr.9b02046.
[233] W. Luo, Q. Liu, Y. Li, S. Zhou, H. Zou, M. Liang, Enhanced mechanical and tribological properties in polyphenylene sulfide/polytetrafluoroethylene composites reinforced by short carbon fiber, Compos. B Eng. 91 (2016) 579–588, https://doi.org/10.1016/j.compositesb.2016.01.036.
[234] Y. Shi, S. Zhou, H. Zou, M. Liang, Y. Chen, In situ micro-fibrillization and post annealing to significantly improve the tribological properties of polyphenylene sulfide/polyamide 66/polytetrafluoroethylene composites, Compos. B Eng. 216 (2021), 108841, https://doi.org/10.1016/J.COMPOSITESB.2021.108841.
[235] D. Wu, Y. Zhang, M. Zhang, L. Wu, Morphology, nonisothermal crystallization behavior, and kinetics of poly(phenylene sulfide)/polycarbonate blend, J. Appl. Polym. Sci. 105 (2007) 739–748, https://doi.org/10.1002/APP.26096.
[236] S. Lim, J. Kim, M. Park, C.R. Choe, J. Lee, D. Kim, Thermal characterization and morphological study of polyphenylene sulfide–polycarbonate blends, Polym. Eng. Sci. 36 (1996) 2502–2508, https://doi.org/10.1002/PEN.10648.
[237] I.S. Bhardwaj, V. Kumar, A. Das, Studies of the thermal and crystallization behaviour of polyphenylene sulphide/polycarbonate blends, Thermochim. Acta 144 (1989) 165–172, https://doi.org/10.1016/0040-6031(89)85095-6.
[238] J. Choi, S. Lim, J. Kim, C.R. Choe, Studies of an epoxy-compatibilized poly (phenylene sulfide)/polycarbonate blend, Polymer (Guildf) 38 (1997) 4401–4406, https://doi.org/10.1016/S0032-3861(96)01032-4.
[239] J.Z. Liang, Heat distortion temperature of PPS/PC blend, PPS/PC nanocomposite and PPS/PC/GF hybrid nanocomposite, J. Polym. Eng. 33 (2013) 483–488, https://doi.org/10.1515/POLYENG-2013-0064/MACHINEREADABLECITATION/RIS.
[240] M. Shibata, R. Yosomiya, Z. Jiang, Z. Yang, G. Wang, R. Ma, Z. Wu, Crystallization and melting behavior of poly(p-phenylene sulfide) in blends with poly(ether sulfone), J. Appl. Polym. Sci. 74 (1999) 1686–1692, https://doi.org/10.1002/(SICI)1097-4628(19991114)74:7<1686::AID-APP11>3.0.CO;2-Q.
[241] M. Lai, J. Liu, Thermal and dynamic mechanical properties of PES/PPS blends, J. Therm. Anal. Calorim. 77 (2004) 935–945, https://doi.org/10.1023/B:JTAN.0000041670.80647.3C/METRICS.
[242] D. Li, G. Qian, C. Liu, D. Wang, C. Chen, X. Zhao, Thermal, morphology, and mechanical properties of polyphenylene sulfide/polyether sulfone binary blends, J. Appl. Polym. Sci. 132 (2015) 41703, https://doi.org/10.1002/APP.41703.
[243] T. Krooß, M. Gurka, V. Dück, U. Breuer, Development of cost-effective thermoplastic composites for advanced airframe structures, in: ICCM International Conferences on Composite Materials, International Committee on Composite Materials, 2015.
[244] L. Sartore, M. Penco, F. Bignotti, I. Peroni, M.H. Gil, M.A. Ramos, A. D'Amore, Reactive reinforcement of the interface of poly(ether sulfone)/poly(phenylene sulfide) polymer blend by PMR-POI, J. Appl. Polym. Sci. 85 (2002) 1297–1306, https://doi.org/10.1002/app.10729.
[245] Y. Yang, B. Li, Y. Zhang, Y. Zhang, G. Zhuang, Thermal and mechanical properties of phenolphthalein polyethersulfone/poly(phenylene sulfide) blends, J. Appl. Polym. Sci. 55 (1995) 633–639, https://doi.org/10.1002/app.1995.070550411.
[246] Z. Chen, T. Li, Y. Yang, X. Liu, R. Lv, Mechanical and tribological properties of PA/PPS blends, Wear 257 (2004) 696–707, https://doi.org/10.1016/j.wear.2004.03.013.
[247] Z. Chen, X. Liu, T. Li, R. Lü, Mechanical and tribological properties of PA66/PPS blend. II. Filled with PTFE, J. Appl. Polym. Sci. 101 (2006) 969–977, https://doi.org/10.1002/app.22061.
[248] N. Bulakh, J.P. Jog, Crystallization of poly(phenylenesulfide)/amorphous polyamide blends: DSC and microscopic studies, J. Macromol. Sci. Phys. 38 (B) (1999) 277–287, https://doi.org/10.1080/00222349908212431.
[249] S. Akhtar, J.L. White, Phase morphology and mechanical properties of blends of poly(p-phenylene sulfide) and polyamides, Polym. Eng. Sci. 32 (1992) 690–698, https://doi.org/10.1002/PEN.760321008.
[250] Z. Su, L. Zeng, S. Zhang, Q. Xu, M. Jiang, J. Liu, C. Wang, P. Liu, The effects of carbon nanotubes selective location on the structures and properties of polyphenylene sulfide/polyamide 66 fibers, J. Appl. Polym. Sci. 139 (2022), https://doi.org/10.1002/app.52214.

[251] H. Zou, N. Ning, R. Su, Q. Zhang, Q. Fu, Manipulating the phase morphology in PPS/PA66 blends using clay, J. Appl. Polym. Sci. 106 (2007) 2238–2250, https://doi.org/10.1002/APP.26880.
[252] K. Mai, Z. Mei, J. Xu, H. Zeng, Effect of blending on the multiple melting behavior of polyphenylene sulfide, J. Appl. Polym. Sci. 63 (1997) 1001–1008, https://doi.org/10.1002/(sici)1097-4628(19970222)63:8<1001::aid-app6>3.3.co;2-i.
[253] R.C. Zhang, Y. Xu, Z. Lu, M. Min, Y. Gao, Y. Huang, A. Lu, Investigation on the crystallization behavior of poly(ether ether ketone)/poly(phenylene sulfide) blends, J. Appl. Polym. Sci. 108 (2008) 1829–1836, https://doi.org/10.1002/app.27725.
[254] C. Jian-Bing, G. Wen-He, L. Zhun-Zhun, T. Li-Ming, Crystalline and thermal properties in miscible blends of PEEK, PPS and PEI obtained by melt compounding, Functional Mater. 23 (2016) 55–62. https://doi.org/10.15407/fm23.01.055.
[255] K.M. Knauer, G. Brust, M. Carr, R.J. Cardona, J.D. Lichtenhan, S.E. Morgan, Rheological and crystallization enhancement in polyphenylenesulfide and polyetheretherketone POSS nanocomposites, J. Appl. Polym. Sci. 134 (2017) 44462, https://doi.org/10.1002/app.44462.
[256] S. Deng, Z. Lin, L. Cao, J. Xian, C. Liu, PPS/recycled PEEK/ carbon nanotube composites: Structure, properties and compatibility, J. Appl. Polym. Sci. 132 (2015), https://doi.org/10.1002/app.42497.
[257] S. Horiuchi, Y. Ishii, Poly(phenylene sulfide) and low-density polyethylene reactive blends, Morphology, tribology, and moldability, Polym. J. 32 (2000) 339–347, https://doi.org/10.1295/polymj.32.339.
[258] S. Nara, K. Watanabe, H.T. Oyama, H. Saito, Control of crystallization in two-phase blends of poly(phenylene sulfide) and poly(vinylpyrrolidone), Polym. Crystallization 4 (2021) e10165.
[259] J. Xing, Q.Q. Ni, B. Deng, Q. Liu, Morphology and properties of polyphenylene sulfide (PPS)/polyvinylidene fluoride (PVDF) polymer alloys by melt blending, Compos. Sci. Technol. 134 (2016) 184–190, https://doi.org/10.1016/j.compscitech.2016.08.020.
[260] Q. Xu, W. Xu, Y. Yang, X. Yin, C. Zhou, J. Han, X. Li, Y. Shang, H. Zhang, Enhanced interlayer strength in 3D printed poly (ether ether ketone) parts, Addit. Manuf. 55 (2022), 102852, https://doi.org/10.1016/j.addma.2022.102852.
[261] A. Diouf-Lewis, R.D. Farahani, F. Iervolino, J. Pierre, Y. Abderrafai, M. Lévesque, N. Piccirelli, D. Therriault, Design and characterization of carbon fiber-reinforced PEEK/PEI blends for Fused Filament Fabrication additive manufacturing, Mater. Today Commun. 31 (2022), 103445, https://doi.org/10.1016/j.mtcomm.2022.103445.
[262] A. Slonov, I. Musov, A. Zhansitov, E. Rzhevskaya, D. Khakulova, S. Khashirova, The effect of modification on the properties of polyetherimide and its carbon-filled composite, Polymers (Basel) 12 (2020) 1056, https://doi.org/10.3390/POLYM12051056.
[263] A. Bagsik, S. Josupeit, V. Schoeppner, E. Klemp, Mechanical analysis of lightweight constructions manufactured with fused deposition modeling, in: AIP Conf Proc, American Institute of Physics Inc., 2014, pp. 696–701. https://doi.org/10.1063/1.4873874.
[264] A. Forés-Garriga, M.A. Pérez, G. Gómez-Gras, G. Reyes-Pozo, Role of infill parameters on the mechanical performance and weight reduction of PEI Ultem processed by FFF, Mater. Des. 193 (2020), 108810, https://doi.org/10.1016/J.MATDES.2020.108810.
[265] R.J. Zaldivar, D.B. Witkin, T. McLouth, D.N. Patel, K. Schmitt, J.P. Nokes, Influence of processing and orientation print effects on the mechanical and thermal behavior of 3D-Printed ULTEM® 9085 Material, Addit. Manuf. 13 (2017) 71–80, https://doi.org/10.1016/J.ADDMA.2016.11.007.
[266] A. Chueca de Bruijn, G. Gómez-Gras, L. Fernández-Ruano, L. Farràs-Tasias, M. A. Pérez, Optimization of a combined thermal annealing and isostatic pressing process for mechanical and surface enhancement of Ultem FDM parts using Doehlert experimental designs, J. Manuf. Process. 85 (2023) 1096–1115, https://doi.org/10.1016/J.JMAPRO.2022.12.027.
[267] G. Mital', I. Gajdoš, E. Spišák, J. Majerníková, T. Jezný, An Analysis of Selected Technological Parameters' Influences on the Tribological Properties of Products Manufactured Using the FFF Technique, Appl. Sci. (Switzerland) 12 (2022) 3853. https://doi.org/10.3390/app12083853.
[268] V.S. Vakharia, H. Leonard, M. Singh, M.C. Halbig, Multi-Material Additive Manufacturing of High Temperature Polyetherimide (PEI)–Based Polymer Systems for Lightweight Aerospace Applications, Polymers (Basel) 15 (2023) 561, https://doi.org/10.3390/polym15030561.
[269] A. Chueca de Bruijn, G. Gómez-Gras, M.A. Pérez, Selective dissolution of polysulfone support material of fused filament fabricated Ultem 9085 parts, Polym. Test. 108 (2022), 107495, https://doi.org/10.1016/J.POLYMERTESTING.2022.107495.
[270] A. Chueca de Bruijn, G. Gómez-Gras, M.A. Pérez, Mechanical study on the impact of an effective solvent support-removal methodology for FDM Ultem 9085 parts, Polym. Test. 85 (2020), 106433, https://doi.org/10.1016/J.POLYMERTESTING.2020.106433.
[271] G.H. Melton, E.N. Peters, R.K. Arisman, Engineering Thermoplastics, Applied Plastics Engineering Handbook: Processing and Materials. (2011) 7–21. https://doi.org/10.1016/B978-1-4377-3514-7.10002-9.
[272] M. Picard, A.K. Mohanty, M. Misra, Recent advances in additive manufacturing of engineering thermoplastics: challenges and opportunities, RSC Adv. 10 (2020) 36058–36089, https://doi.org/10.1039/D0RA04857G.
[273] C.A. Chatham, C.E. Zawaski, D.C. Bobbitt, R.B. Moore, T.E. Long, C.B. Williams, Semi-Crystalline Polymer Blends for Material Extrusion Additive Manufacturing Printability: A Case Study with Poly(ethylene terephthalate) and Polypropylene, Macromol. Mater. Eng. 304 (2019), https://doi.org/10.1002/MAME.201800764.